



Research paper

Antibacterial and antibiofilm activity of permanently ionized quaternary ammonium fluoroquinolones



Joanna Fedorowicz^{a,b,*}, Cristina D. Cruz^b, Małgorzata Morawska^{a,b,c}, Krzesimir Ciura^{d,e}, Shella Gilbert-Girard^b, Liliana Mazur^f, Heidi Mäkylä^b, Polina Ilina^b, Kirsi Savijoki^{g,h}, Adyary Fallarero^b, Päivi Tammela^b, Jarosław Sączewski^c

^a Department of Chemical Technology of Drugs, Faculty of Pharmacy, Medical University of Gdańsk, Al. Gen. J. Hallera 107, 80-416, Gdańsk, Poland

^b Drug Research Program, Division of Pharmaceutical Biosciences, Faculty of Pharmacy, University of Helsinki, P.O. Box 56 (Viikinkaari 5E), FI-00014, Helsinki, Finland

^c Department of Organic Chemistry, Faculty of Pharmacy, Medical University of Gdańsk, Al. Gen. J. Hallera 107, 80-416, Gdańsk, Poland

^d Department of Physical Chemistry, Faculty of Pharmacy, Medical University of Gdańsk, Al. Gen. J. Hallera 107, 80-416, Gdańsk, Poland

^e QSAR Lab Ltd., Trzy Lipy 3 St., 80-172, Gdańsk, Poland

^f Institute of Chemical Sciences, Faculty of Chemistry, Maria Curie-Skłodowska University, Plac Marii Curie-Skłodowskiej 5, 20-031, Lublin, Poland

^g Infection Biology, Faculty of Medicine and Health Technology, Tampere University, Kalevantie 4, FI-33100, Tampere, Finland

^h Department of Food and Nutrition, Faculty of Agriculture and Forestry, University of Helsinki, Agnes Sjöbergin katu 2, P.O. Box, FI-00014, Helsinki, Finland

ARTICLE INFO

Keywords:

Antibacterial activity
Antibiofilm activity
Molecular docking
Pseudomonas aeruginosa
Quaternary ammonium compounds
Quinolone

ABSTRACT

A series of quaternary ammonium fluoroquinolones was obtained by exhaustive methylation of the amine groups present at the 7-position of fluoroquinolones, including ciprofloxacin, enoxacin, gatifloxacin, lomefloxacin, and norfloxacin. The synthesized molecules were tested for their antibacterial and antibiofilm activities against Gram-positive and Gram-negative human pathogens, i.e. *Staphylococcus aureus* and *Pseudomonas aeruginosa*. The study showed that the synthesized compounds are potent antibacterial agents (MIC values at the lowest 6.25 µM) with low cytotoxicity *in vitro* as assessed on the BALB 3T3 mouse embryo cell line. Further experiments proved that the tested derivatives are able to bind to the DNA gyrase and topoisomerase IV active sites in a fluoroquinolone-characteristic manner. The most active quaternary ammonium fluoroquinolones, in contrast to ciprofloxacin, reduce the total biomass of *P. aeruginosa* ATCC 15442 biofilm in post-exposure experiments. The latter effect may be due to the dual mechanism of action of the quaternary fluoroquinolones, which also involves disruption of bacterial cell membranes. IAM-HPLC chromatographic experiments with immobilized artificial membranes (phospholipids) showed that the most active compounds were those with moderate lipophilicity and containing a cyclopropyl group at the N1 nitrogen atom in the fluoroquinolone core.

1. Introduction

Antimicrobial resistance is a problem of increasing global concern. In particular, the ESCAPE pathogens, including *Enterococcus faecium*, *Staphylococcus aureus*, *Klebsiella pneumoniae*, *Acinetobacter baumannii*, *Pseudomonas aeruginosa*, and *Enterobacter* species, are the most threatening due to their multidrug resistance against common antibiotics and/or to the ability to form antibiotic-tolerant biofilms. This fact highlights the need for a renewed and more coordinated research effort in the fight against antibacterial resistance by both the pharmaceutical industry and academia [1–9].

Fluoroquinolones (FQs) are antibacterial agents that play a substantial role in combating urinary tract infections, chronic prostatitis, acute pyelonephritis, as well as community-acquired pneumonia [10–13]. This class of bactericides inhibits bacterial type II topoisomerases such as DNA gyrase and topoisomerase IV, which catalyze changes in DNA topology by cleavage and re-joining double-stranded nucleic acids at the phosphate backbone linkage to remove the torsion. Quinolones include four generations of drugs that share 4-quinolone or related bicyclic core structure (Fig. 1). Carboxyl and carbonyl groups in C3 and C4 positions, respectively, are essential for binding to the enzyme by the formation of a hydrogen bond with the hydroxyl group of serine residue and chelation to a magnesium ion. In positions N1 and C2

* Corresponding author. Department of Chemical Technology of Drugs, Faculty of Pharmacy, Medical University of Gdańsk, Al. Gen. J. Hallera 107, 80-416, Gdańsk, Poland.

E-mail address: jfedorowicz@gumed.edu.pl (J. Fedorowicz).

<https://doi.org/10.1016/j.ejmech.2023.115373>

Received 23 January 2023; Received in revised form 29 March 2023; Accepted 11 April 2023

Available online 14 April 2023

0223-5234/© 2023 The Authors. Published by Elsevier Masson SAS. This is an open access article under the CC BY license (<http://creativecommons.org/licenses/by/4.0/>).

Abbreviations

ACN	acetonitrile;
ATCC	American type culture collection
BBB	blood-brain barrier
CC ₅₀	cytotoxic concentration
CFU	colony-forming unit
CHI	chromatographic hydrophobicity index
CLSI	Clinical and Laboratory Standards Institute
CNS	central nervous system
DMF	dimethylformamide;
DMSO	dimethyl sulfoxide;
FBS	fetal bovine serum
FQ	fluoroquinolone
GI	gastrointestinal tract
HPLC	high-performance liquid chromatography
IAM	immobilized artificial membrane
LC-MS	liquid chromatography-mass spectrometry

MBEC	minimum biofilm eradication concentration
MBIC	minimum biofilm inhibition concentration
MHA	Mueller Hinton agar
MHB	Mueller Hinton broth
MIC	minimum inhibitory concentration
NBCS	newborn calf serum
OD	optical density
PBS	phosphate-buffered saline;
QAC	quaternary ammonium compound
rpm	revolutions per minute
RT	room temperature
SD	standard deviation
SI	selectivity index
TLC	thin-layer chromatography
TPSA	topological polar surface area
TSA	tryptic soy agar
TSB	tryptic soy broth
WLOGP	Wildman and Crippen logP model

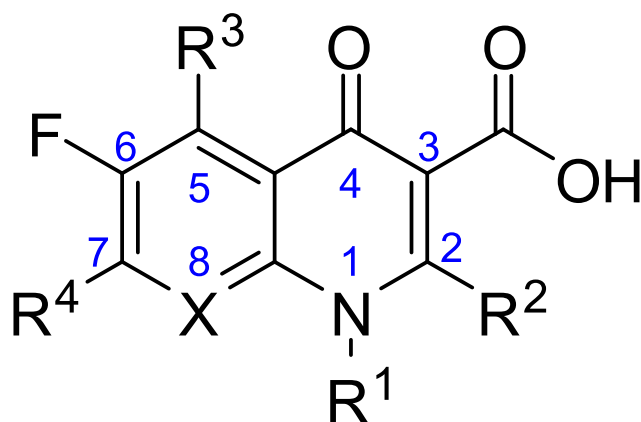


Fig. 1. The general structure of fluoroquinolones.

only small substituents are allowed to sustain the activity. Usually, hydrogen atom and ethyl or cyclopropyl groups can be found as R² and R¹ substituents, respectively. The fluorine atom present in the C6 position affects the potency [14]. The introduction of bulky substituents is permitted only at the C7 position since it significantly influences the effectiveness, spectrum of activity, and safety of a drug [15,16]. Furthermore, it may result in a reduction of resistance development as well as susceptibility to the bacterial efflux pump system [17–19]. FQs can be administered both orally and intravenously. They are easily distributed in the human organism which allows to attain effective concentrations in most of the tissues. It is assumed that FQs penetrate cells by passive permeation of lipid bilayers [20,21] or facilitated diffusion through porin channels [22,23] which is conditioned by interconversion between ionized and uncharged forms in equilibrium [24–26]. Interestingly, FQs constitute also one of the most extensively utilized groups of compounds employed for the synthesis of hybrid drugs [27–32].

Quaternary ammonium compounds (QAC) are permanently charged salts that are commonly used as surfactants, disinfectants, antistatic agents etc [33]. They act as antibacterials by disrupting the cell membrane of microorganisms. Moreover, introduction of a quaternary ammonium functionality to a biologically active molecule may result in increased water solubility and reduced blood-brain barrier (BBB) penetration [34–36].

Recently, we have synthesized FQ-*Safirinium* dye hybrids conjugated at the C7 position with a large pyrrodo-triazolinium system. We confirmed our original hypothesis that for high molecular weight FQ hybrids with quaternized piperazinyl moieties, it is lipophilicity [37] and not steric factors that limits the antibacterial activity of FQ [38–40]. These findings prompted us to verify the prevailing assumption that FQs bearing permanent positive charge exhibit weak antibacterial activity [41]. Therefore we proposed a series of quaternary ammonium FQs to evaluate their physicochemical properties along with their antibacterial, antibiofilm and cytotoxic effects. The presence of permanent charges on the nitrogen atoms within the structures, in addition to hindered penetration into the bacterial cell, should cause interference with the lipid bilayer of the cytoplasmic membrane of bacteria and the outer membrane of Gram-negative bacteria, prevent distribution to the brain, and as a result, the compounds should not cause direct side effects from the central nervous system (CNS) after intravenous administration [42,43].

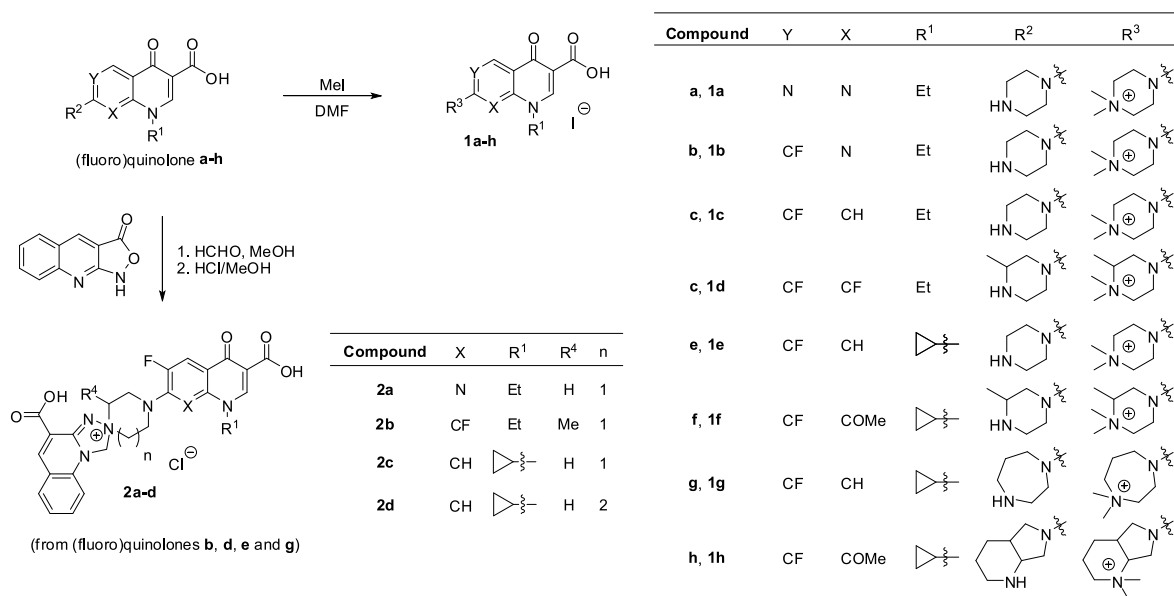
2. Results and discussion

2.1. Chemistry

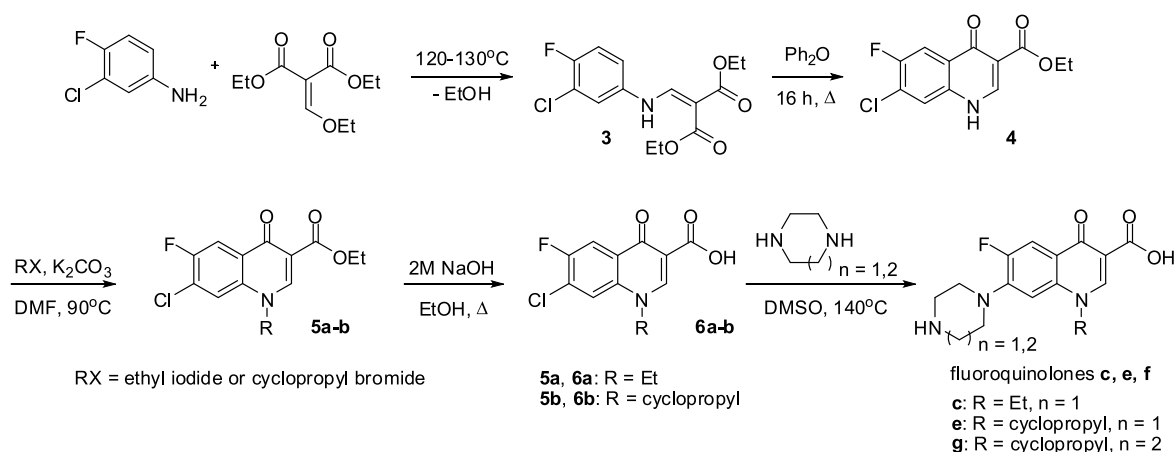
2.1.1. Design and synthesis

Typically, a FQ features a cyclic amine, such as 6-membered ring piperazine, at the C7 position of the fused bicyclic structure. We have designed a series of new dimethyl quaternary ammonium derivatives 1a-h (Scheme 1) which were obtained through alkylation of the terminal aliphatic nitrogen atom present in the C7 heterocyclic substituent. The test set was extended with four hybrid compounds 2a-d (Scheme 1) in order to compare the antibacterial potencies with the previously assessed dual-acting molecules (FQ-*Safirinium* hybrids) [38].

FQ-core intermediates were synthesized *via* the multi-step route from 3-chloro-4-fluoroaniline (Scheme 2) according to the procedure reported in the literature [44,45]. Briefly, 3-chloro-4-fluoroaniline was reacted with diethyl 2-(ethoxymethylene)malonate to afford the crude malonate 3, which was further transformed into 7-chloro-6-fluoro-4-oxo-1,4-dihydroquinoline-3-carboxylic acid ethyl ester 4. The latter compound was subjected to *N*-alkylation reactions with alkyl halides in the presence of anhydrous potassium carbonate to obtain 1-alkyl-1,4-dihydro-4-oxoquinoline esters 5a-b. The esters were hydrolyzed with sodium hydroxide to produce the carboxylic acids 6a and 6b, which were subsequently reacted with piperazine or homopiperazine to provide the corresponding 7-amino products c (norfloxacin), e (ciprofloxacin) and g. The remaining (fluoro)quinolones a (pипemidic acid), b (enoxacin), d (lomefloxacin), 1f (gatifloxacin), and h (moxifloxacin)



Scheme 1. The synthesis of N-quaternized quinolones 1 and 2.



Scheme 2. Synthesis of intermediates c, e and f.

were commercially acquired.

The scheduled dimethyl quaternary ammonium derivatives 1a-h were synthesized from the obtained intermediates 7a-c as well as commercially available FQ antibiotics via exhaustive alkylation with methyl iodide (Scheme 1). The hybrid FQs 2a-d were obtained through the tandem Mannich – electrophilic amination reactions with the use of FQs and profluorophoric isoxazolo[3,4-b]quinolin-3(1H)-one in the presence of formaldehyde and subsequently converted into hydrochlorides (Scheme 1). The structures of all compounds were verified by spectral data, i.e. IR, HRMS, and NMR (Figs. S1–S23 and elemental analysis). The structure of compound 1e was additionally characterized using X-ray crystallography (Fig. 2). Single crystals of derivative 1e, suitable for X-ray diffraction studies, were obtained after recrystallization of the resulting product from dry methanol, using standard slow solvent evaporation technique.

The compound crystallizes in the monoclinic space group $P2_1/c$. The asymmetric unit in the crystal consists of one quaternized ciprofloxacin cation, one iodide anion, and two water molecules. The molecular plot for the studied structure with the atom-labelling scheme is shown in Fig. 2, whereas the relevant geometric parameters are given in Table S1.

2.1.2. ADME/Tox profile

Theoretical estimation of pharmacokinetics and toxicological properties can help to assess the potency of drug candidates, especially in the preclinical stages of drug development. The free available SwissADME web-based application developed and maintained by the Molecular Modelling Group of the Swiss Institute of Bioinformatics (<http://www.swissadme.ch>) was utilized to realize this purpose. The software allows for rapid prediction of several essential ADME properties, including adsorption, metabolism penetration through the BBB, and calculation of drug-likeness or physicochemical properties. All the calculated properties are collected in supplementary materials in Table S3. All the investigated molecules were characterized with high gastrointestinal tract (GI) absorptions. The predictions indicated that the tested compounds are soluble, ranging between moderately soluble and soluble by means of the methods proposed by Ali [46]. Oppositely, only one molecule (1d) can penetrate through BBB. Taking into account the adverse reactions of the central nervous system during therapy with FQs [47], cerebral uptake should be considered one of the most important aspects of the assessment of the newly synthesized FQ derivatives. The “BOILED-egg” plot presented in Fig. 3 summarized and visualized the human gastrointestinal absorption and BBB permeability of target molecules using the 2D space created by two molecular descriptors,

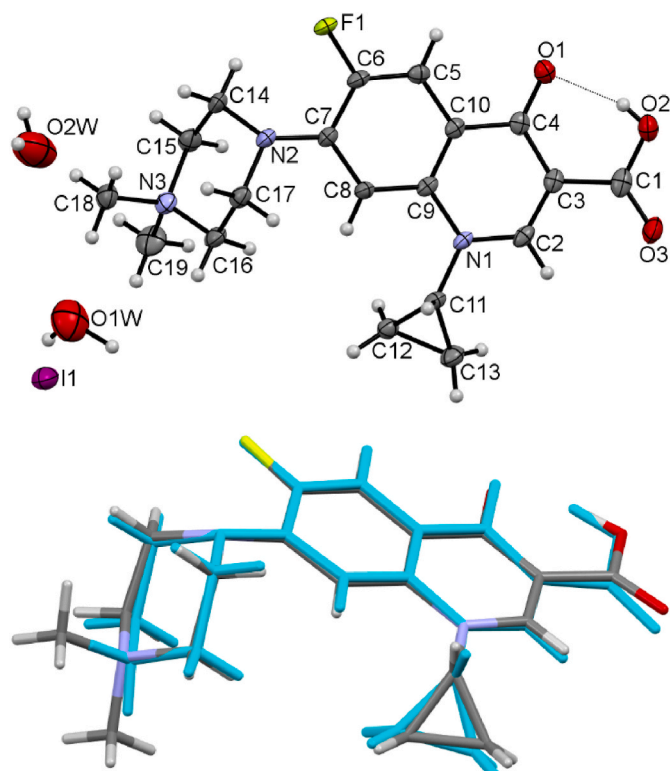


Fig. 2. Upper panel: the perspective view of the asymmetric unit in crystal **1e** with labelling of atoms and estimation of their thermal motion parameters as ADPs (ellipsoids are at the 50% probability level); dashed line indicates intramolecular hydrogen bond. Lower panel: an overlay of the cations present in crystal **1e** (grey line) and ciprofloxacin hydrochloride (CSD refcode: MUGCID01 [36]) (blue line).

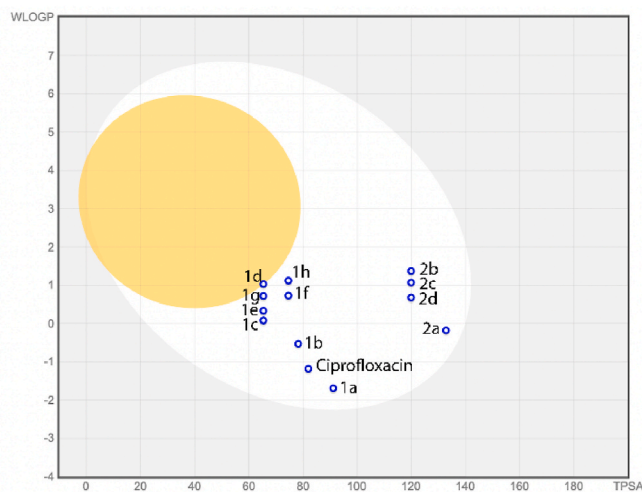


Fig. 3. The GI tract and BBB passive penetration parameters estimated for the studied molecules by the BOILED-Egg scheme. The compounds absorbed after oral administration are gathered in the white egg area, while those penetrating the BBB should be in the yolk region.

Wildman and Crippen logP model (WLOGP) and topological polar surface area (TPSA). Additionally, all the investigated compounds along with ciprofloxacin scored 0.55 or 0.56 in the bioavailability model, which suggests desirable pharmacokinetic properties. SwissADME provides five different rule-based filters developed initially by major pharmaceutical companies such as Lipinski (Pfizer), Ghose (Amgen),

Veber (GSK), Egan (Pharmacia), and Muegge (Bayer) filters [48–51]. Generally, the target derivatives meet all the criteria, except for derivatives **2a–2d**, which exceeded limits for molecular weight and molar refractivity indices according to Lipinski and Ghose ($MR > 130$), respectively. Additionally, derivatives **1a,b** did not meet Ghose criteria since their WLOGP estimates were lower than -0.4 . However, the market-available ciprofloxacin proved a violation at the same point.

2.1.3. Physicochemical properties

According to the calculated lipophilicity indices, all the tested compounds should be considered hydrophilic. Nevertheless, significant differences between the calculated logP parameters depending on the algorithms used should be emphasized (Table S3). For this reason, the experimental protocol engaging immobilized artificial membrane chromatography (IAM-HPLC) was also applied to characterize the physicochemical properties of the tested FQ derivatives. Presently, automated chromatographic approaches are widely used in drug discovery to determine physicochemical properties, while the IAM-HPLC approach provides the benefit of more biomimetic stationary phase compared to the classical *n*-octanol system. Hence, the affinity to phospholipids has been evaluated by means of experimental chromatographic hydrophobicity index (CHI) determinations according to the method originally proposed by Valko [52] and later validated by pharmaceutical companies such as GSK. The results obtained are presented in Table S3. The lowest affinities for artificial membranes were shown by the pipemidic acid analog **1a** ($CHI_{IAM} = 1.60$), as well as the enoxacin-based hybrid containing the 1,8-naphthyridine core **2a** (3.90). Slightly higher phospholipophilicity indices were observed for quaternized enoxacin **1b** (8.75), lomefloxacin **1d** (7.66), and hybrid ciprofloxacin **2c** (7.55). Then, quaternized norfloxacin **1c** (13.41), ciprofloxacin **1e** (12.17), and gatifloxacin **1f** (11.7), as well as ciprofloxacin hybrid **2d** (13.72) demonstrated moderate hydrophobicity indices, while quaternized ciprofloxacin analogue **1g** (18.23), moxifloxacin **1h** (22.27), and hybrid lomefloxacin **2b** (15.44) proved values comparable to that of unmodified ciprofloxacin (19.7).

2.2. In vitro biological evaluation

2.2.1. Antibacterial activity

The conducted microbiological experiments provided data on the antibacterial potential of the synthesized compounds. The molecules were tested against two biofilm-forming bacterial strains that cause infections in humans, Gram-negative *Pseudomonas aeruginosa* and Gram-positive *Staphylococcus aureus*. Ciprofloxacin hydrochloride was used as a reference compound. Initially, the compounds were screened at a concentration of 50 μ M (Table S4). Minimum inhibitory concentration (MIC) values were determined for derivatives that exhibited above 80% of growth inhibition in the screening assays. The determined data for the active compounds are summarized in Table 1. The antibacterial data for compounds **2a–c** have been reported previously [38].

Compounds **1e** and **1g** were found to be the most effective towards both tested bacteria and presented MIC values in the low micromolar range. Compound **1f** was selectively active towards *S. aureus* strain (*i.e.* MIC of 6.25 μ M), while hybrid **2d** was active against both strains at moderately higher concentration (*i.e.* MIC of 25 μ M).

2.2.2. Antibiofilm activity

S. aureus and *P. aeruginosa* are known for their ability to form biofilms, which can be formed on the surface of urinary catheters, medical implants, chronic wounds, and in the lungs of cystic fibrosis patients [53]. Thus, it is of clinical interest that inhibitory concentrations of novel antibacterials are also tested on biofilms and not just on planktonic cells.

In order to assess the potential against pathogenic bacteria, all the synthesized compounds were subjected to antibiofilm assays with ciprofloxacin used as a control [54,55,56]. Firstly, their activity was

Table 1

Minimum Inhibitory Concentration^a [μM] of compounds **1b-h** and **2d** against *P. aeruginosa* and *S. aureus* bacterial strains.

Compound	<i>Pseudomonas aeruginosa</i> ATCC 27853	<i>Staphylococcus aureus</i> ATCC 29213
1a	>50	>50
1b	>50	50
1c	>50	25
1d	75	25
1e	6.25	6.25
1f	>50	6.25
1g	6.25	6.25
1h	>50	50
2d	25	25
Ciprofloxacin hydrochloride	2.72	1.36

^a Minimum Inhibitory Concentration was defined as the concentration of compound that inhibited bacterial growth by $\geq 90\%$. If during the screening testing the threshold of 80% of growth inhibition was not achieved, the value is represented by the highest concentration of compound tested.

screened in pre- and post-exposure to investigate whether they were able not only to prevent the formation but also eradicate pre-existing biofilm. Full results are available in the Supplementary material (Figs. S26–S41). Compound **1e** was the most active against *P. aeruginosa* (Figs. S36 and S37). Also compounds **1g** and **2a,c** were highly potent and inhibited above 90% of biofilm viability and total biomass at the concentrations of 20–40 and 40–80 μM , respectively. What is more, ciprofloxacin derivative **1e** exhibited the strongest effect in *S. aureus* biofilm formation prevention (Figs. S28 and S29). Compounds **1f,g** and **2a-c** were also

active and inhibited above 90% of biofilm growth at concentrations of 2.5–5 μM . In addition, compound **1f** was the most active in the eradication of mature biofilm of this strain (Figs. S32 and S33).

Based on these results, compounds **1e,g** and **2d** were selected for further studies on *P. aeruginosa* while **1e-g** were additionally evaluated against *S. aureus* (Figs. 4–6). It should be noted that all the above selected FQ antibacterial agents featured a cyclopropyl ring at the N1 position and proved moderate phospholipophilicity indices in the range of 11.70–18.23.

Noticeable trends in reduction of biofilm formation by compounds **1e** and **1g** can be observed from 5 μM reaching above 90% at the concentration of 25 μM , while compound **2d** proved *P. aeruginosa* biofilm inhibition above the concentration of 25 μM (at 100 μM , i.e. the highest concentration tested, the biofilm viability was reduced by 80%). The total biomass measurements revealed similar tendencies, however, some differences can be observed. The minimum biofilm inhibitory concentration (MBIC) for compounds **1e** and **1g** achieved in the viability assay was 25 μM , while the value determined in the total biomass assessment was one dilution step higher, that is 50 μM (Fig. 4).

Further experiments in the post-exposure mode revealed a significant reduction of a mature biofilm. Minimum biofilm eradication concentration (MBEC) values have not been reached up to the highest concentration tested (200 μM), however, a decrease in cell viability can be observed in comparison to untreated cells. The degradation of approximately 50% of pre-formed biofilm in the viability assay can be observed at 10 and 50 μM for compounds **1e,g**, and **2d**, respectively; nevertheless, the total biomass assessment has not revealed any significant changes and only some minor reduction was observed. The most noteworthy observation is that ciprofloxacin has no effect on the biomass of mature

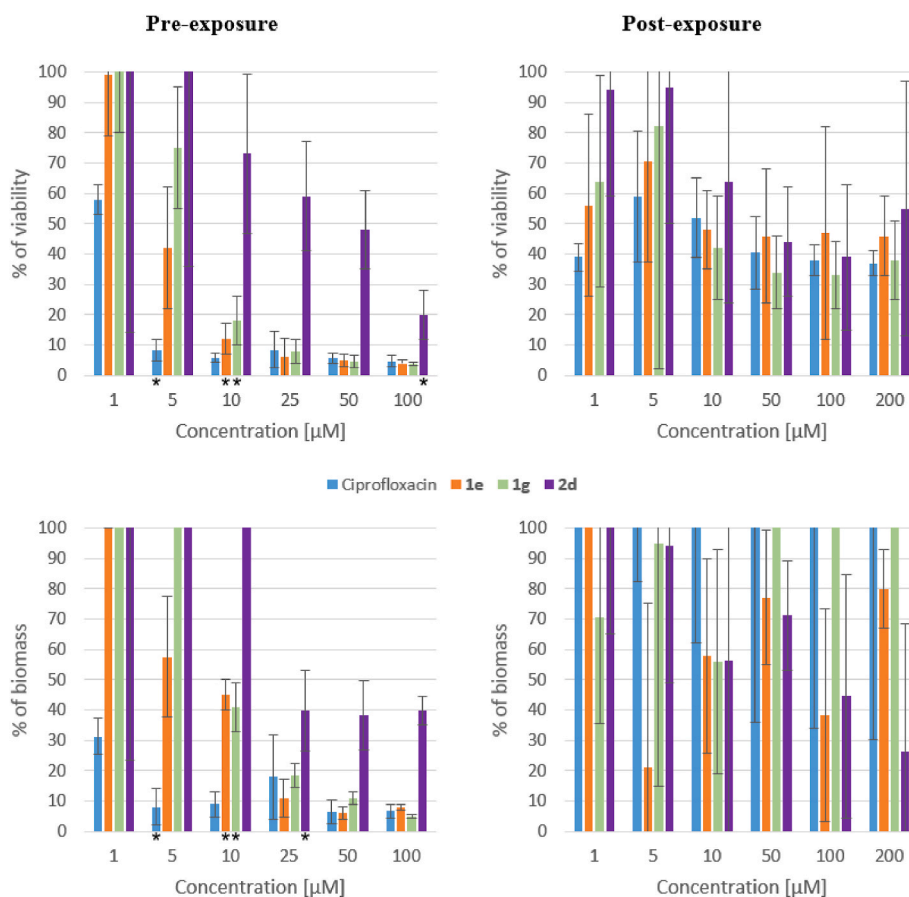


Fig. 4. The effect of the most active derivatives on *P. aeruginosa* ATCC 15442 biofilm formation in pre-exposure (left panel) and post-exposure (right panel): viability (upper panel) and total biomass (lower panel) assessment. The results are expressed as a percentage relative to the untreated controls (100%) \pm SD. Two biological experiments were performed with two technical replicates for each condition. The statistical significance $p < 0.05$ was marked with *.

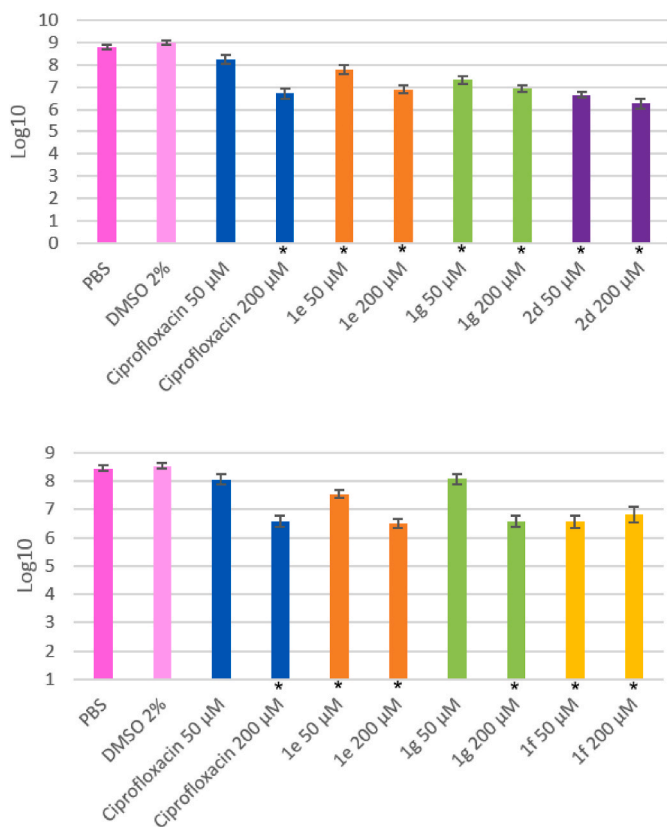


Fig. 5. Reduction of the viable cells in *P. aeruginosa* (upper panel) and *S. aureus* (lower panel) biofilms after treatment with the compounds in post-exposure. Results are expressed as the log₁₀ of the number of cells per mL obtained by CFU count \pm SD. Results are from 2 different experiments performed on different days with 2 technical replicates for each condition. The statistical significance $p < 0.05$ was marked with *.

P. aeruginosa biofilms, which underlines the beneficial role of the quaternary ammonium moiety present in the modified FQs (Fig. 4). It is generally recognized that numerous bacterial cells inside a mature biofilm enter a dormant stage where their metabolic activity is nearly or completely inexistent, especially when exposed to antimicrobials. These inactive cells cannot be detected by resazurin staining but they are still viable. Dormant cells can start to grow and multiply again when more favorable conditions occur. Therefore, in order to quantify the activity of quinolones **1e,g**, and **2d** in terms of viable cells reduction, colony-forming unit (CFU) count was performed on mature biofilms treated post-exposure. At 200 μ M, the tested compounds caused a 2-log reduction of the CFU (Fig. 5).

These results showed that compounds **1e,g**, and **2d** were as effective or better than ciprofloxacin in reducing the number of viable cells in mature biofilms. In particular, compound **2d** at a concentration of 50 μ M was as efficient as ciprofloxacin at a concentration of 200 μ M.

The results of the most active compounds **1e-g** against *S. aureus* biofilms are presented in Fig. 6. Hence, compound **1f** most effectively inhibits biofilm in pre-exposure experiments. Its activity against *S. aureus* is comparable to that of ciprofloxacin – the MBIC was assessed at 5 μ M, which is at the same concentration as determined for ciprofloxacin. Compounds **1e** and **g** elicit approximately 100% inhibition at 10 μ M. Moreover, compound **1f** was the most effective in post-exposure tests – its activity at a concentration of 10 μ M is comparable to that of the reference drug, ciprofloxacin. Derivatives **1e** and **1g** reach maximal inhibition of the pre-formed biofilm viability (ca. 60–70%) at 50 μ M. Again, the total biomass measurements have not provided any significant differences (Fig. 6). Then, quantification of viable cells in the biofilm was performed. The results confirmed that derivative **1f** was the

most effective at reducing the number of viable cells in mature biofilms. Thus, quinolone **1f** achieved a 2-log reduction at a concentration of 50 μ M, while ciprofloxacin and derivatives **1e** and **1g** showed comparable activities and reduced the amount of CFU by 2 logs at concentrations of 200 μ M (Fig. 5).

2.2.3. Cytotoxicity studies

The cytotoxicity of the most active compounds **1e-g** and **2d** was examined at the concentrations of 50 and 200 μ M in mouse embryonic fibroblasts BALB/3T3 clone A31 using the luminescent ATP-based CellTiter-Glo® cell viability assay [57]. None of the tested compounds were found to be toxic up to 50 μ M (Table S5). At 200 μ M, compounds **1f,g** and ciprofloxacin caused circa 30, 20, and 15% decrease in cell viability, respectively, while hybrid **2d** was highly cytotoxic showing less than 2% viable cells. However, the determined 50% cytotoxicity concentration (CC₅₀) value for the latter compound was nearly 160 μ M, which is considerably higher than the MIC value of 25 μ M giving the selectivity index (SI) of 6.4. The SI values calculated for the other active compounds were above 32, which proves their safety in mammals (Table 2).

2.3. Molecular docking studies

The molecular mechanism of FQ action involves inhibition of bacterial type II topoisomerases activity. This class of proteins constitutes well-established and clinically validated targets for drug discovery since these enzymes are essential for DNA replication, transcription, and recombination. DNA gyrase is responsible mainly for the relaxation of the positive supercoils in the DNA molecule by causing negative supercoiling, whereas topoisomerase IV is involved primarily in positive supercoils relaxation and decatenation of the two daughter chromosomes prior to cell division. Both enzymes are heterotetrameric homologous proteins consisting of two GyrA and two GyrB (A₂B₂) or two ParC and two ParE (C₂E₂) subunits, respectively. GyrA and ParC are responsible for binding and transit of DNA, whereas GyrB and ParE contain ATP-binding domain and provide energy for the conformational movements of the enzyme, required for the ligation process [58]. The FQ drug stabilize the DNA-enzyme cleavage complex in Mg²⁺-dependent mode which was confirmed by the crystal structure of moxifloxacin in complex with *Acinetobacter baumannii* topoisomerase IV [59]. The aromatic core of the drug molecule interferes with nucleobases and is anchored by drug-specific protein contacts, principally via a hydrogen bond formed between the C3-carboxyl group of quinolone and hydroxyl group of a conserved serine residue in the DNA cleavage domain. The fluorine atom present in later generations of fluoroquinolones is optimal for drug activity and interacts via the electronegative attraction with partially charged atoms in the DNA bases [60,61].

To investigate the interactions of the novel compounds with the topoisomerases catalytic sites and rationalize the observed antimicrobial action, docking experiments were performed. Crystal structures of enzyme-DNA complexes were obtained from the Protein Data Bank [62]. DNA gyrase and topoisomerase IV from *S. aureus* and *S. pneumoniae*, respectively (PDB codes: 5cdq [63] and 3rae [64]) were used for modeling, since appropriate crystal structure for *P. aeruginosa* was not available in PDB database. The ligands in ionized form together with ciprofloxacin as a reference compound were docked using OpenEye software [65]. All the novel quaternary ammonium FQs were able to interact with both active centers of the enzymes in the FQ-binding manner. In all cases hydrogen bond was formed between serine side chain (Ser84 in *S. aureus* GyrA and Ser79 in *S. pneumoniae* ParC) and the carboxylate oxygen atom present in the quinolone scaffold. The carboxylate and carbonyl oxygen atoms of quinolone chelated a magnesium ion coordinated in the active site. The wedge-shaped core of the quinolones was stacked between DNA base pairs at the cleavage site and stacking interactions of π - π type were created. Overall, the ligands adhered tightly in the active pocket, and the binding was supported by

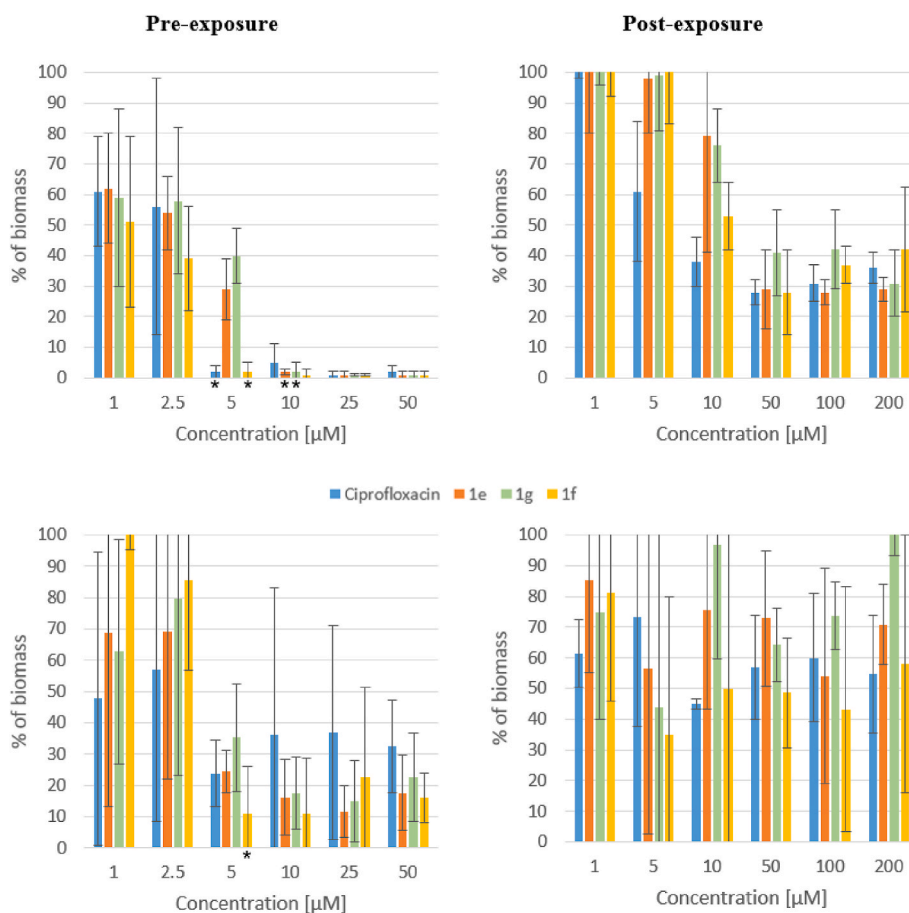


Fig. 6. The effect of the most active derivatives on *S. aureus* ATCC 25923 biofilm formation in pre-exposure (left panel) and post-exposure (right panel): viability (upper panel) and total biomass (lower panel) assessment. The results are expressed as a percentage relative to the untreated controls (100%) \pm SD. Two biological experiments were performed with two technical replicates for each condition. The statistical significance $p < 0.05$ was marked with *.

Table 2

The results of cytotoxicity assays for compounds **1e**, **1f**, **1g**, and **2d**.

Compound	Viability at 200 μ M (%)	CC ₅₀ [μ M]	SI
1e	108.02 \pm 14.02	>200	>32 ^a
1f	70.32 \pm 3.95	>200	>32 ^b
1g	81.68 \pm 3.31	>200	>32 ^a
2d	1.55 \pm 0.22	159.92 \pm 9.23	6.4 ^a
Ciprofloxacin hydrochloride	85.76 \pm 2.66	>200	>147.0 ^b ; >73.5 ^c

^a Calculated for both strains.

^b Calculated for *S. aureus*

^c Calculated for *P. aeruginosa*

additional van der Waals interactions. In several cases, attractive charge contacts were detected between the positively charged nitrogen atom and glutamic or aspartic acid residues of GyrB/ParE subunits. What is more, no charge repulsions in almost all docked ligands were detected as it was seen previously for *Safirinium* hybrids [38]. As observed in the preceding study, the carboxylic acid group present in the *Safirinium* part of the conjugate showed unfavorable interactions with acidic groups of the abovementioned glutamic or aspartic acid of GyrB/ParE subunits.

The most active compounds **1e** and **1g** were ranked highest among all docked ligands (Chemgauss4 scores of -19.72 and -18.49 for the top ranked poses, respectively) in the topoisomerase IV binding pocket, *i.e.* higher than the reference compound ciprofloxacin (-18.87) and lower only than the original ligand, levofloxacin (-19.95) (Table S6). The

active derivative **1f** was ranked slightly lower than ciprofloxacin with the Chemgauss4 score of -18.78 . The molecular structure of the most active derivatives **1e** and **1g** docked in the active pocket of the analyzed enzyme is presented in Fig. 7 while the 2D diagrams of interactions are included in Supplementary material (Figs. S42 and S44). The compounds form hydrogen bonds between the hydroxyl group of Ser79 and the carboxylate group of quinolone with lengths ranging from 2.9 to 3.3 Å. This value is consistent with the experimentally determined distances of the original drug found in crystal structure (2.8 and 3.4 Å). Both active ligands **1e** and **1g** form van der Waals interactions with Arg117 from ParC as well as Arg456, Gly457, and Glu474 from ParE subunits. Compound **1e** interacts additionally with Tyr118 from ParC. Similar results, involving van der Waals interactions with Arg456 and Gly457, were observed for active compounds **1f** and **2d**. However, these ligands proved also attractive charge interactions between guanidine residue Arg117 and carboxylate group of fluoroquinolone core as well as carboxylate Glu474 group and the quaternary nitrogen atom (Figs. S43 and S46). Nevertheless, in the case of ligand **2d** the latter residue forms unfavorable bump with carboxylate group of *Safirinium* part due to repulsion of negative charges.

In the DNA gyrase binding pocket compound **1h** (moxifloxacin derivative) was ranked higher than the original ligand moxifloxacin (Chemgauss4 score of -23.23 versus -22.14). The active compounds **1f** and **1g** were ranked only slightly lower than the original ligand (-21.68 and -21.42 , respectively), while ligands **1e** and **2d** achieved Chemgauss4 scores of -20.84 and -20.03 , respectively, and therefore were superior to the reference ciprofloxacin (-19.72). The highest ranked poses of compounds **1e** and **1g** docked in this enzyme are presented in

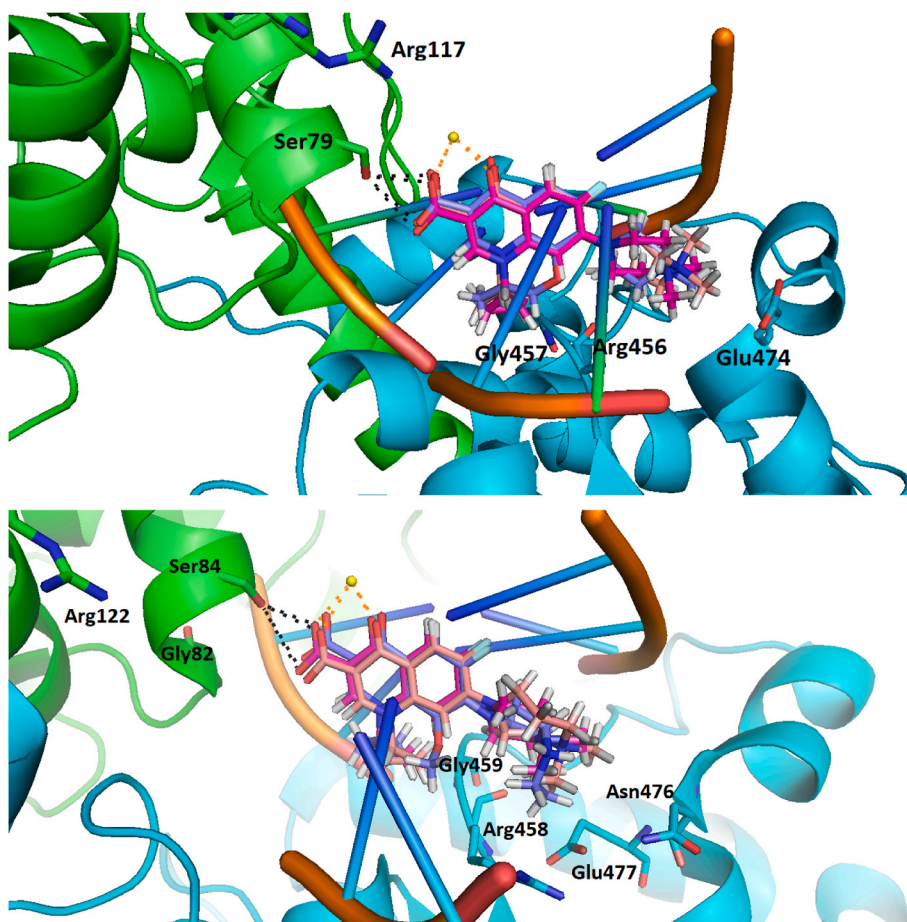


Fig. 7. The highest scored poses of compound **1e** and **1g** (magenta and lightpink sticks) docked in the cleavage site of *S. pneumoniae* topoisomerase IV (upper panel) and *S. aureus* DNA gyrase (lower panel). Magnesium ion as a yellow sphere; subunits GyrA/ParC and GyrB/ParE in green and cyan, respectively; original ligands from crystal structures, moxifloxacin and levofloxacin, respectively, in blue sticks. For clarity, only relevant amino acids are presented. Metal-acceptor and hydrogen bonds are indicated as orange and black dotted lines. The Figure was prepared by PyMOL 1.5.0.3. (For interpretation of the references to color in this figure legend, the reader is referred to the Web version of this article).

Fig. 7. The lengths of hydrogen bonds between the carboxylate group of quinolone and the hydroxyl group of Ser84 are in the range of 2.6–3.9 Å (2.9 and 3.1 Å for the original ligand). Both structures form additional hydrogen bonds between carboxylate group and Arg122 from GyrA. Cyclopropyl ring of compound **1g** form hydrophobic contacts with alkyl chain of Arg458, while compound **1e** presents van der Waals interactions with Gly82 from GyrA as well as Arg458, Gly459, Asn476, and Asn477 from GyrB subunits. Compound **1f** interact similarly to **1e** and forms interactions of the same type with the only exception for Arg122 – in this case, attractive charge interactions were detected. In addition, van der Waals contacts with Asp437 (GyrB subunit) were identified for this ligand. Finally, docking of compound **2d** revealed van der Waals interactions with Gly459, Asn476, and Glu477 as well as charge interactions with Arg122 and Arg458. Nonetheless, the latter residue creates favorable cation- π contacts with aromatic core of *Safirinium* part and unfavorable bump with quaternary nitrogen atom.

2.4. Summary discussion

Studies have shown that FQs can enter Gram-positive bacterial cells through passive diffusion, but only the neutral form of the compounds is believed to cross the cytoplasmic membrane [66,67]. In contrast, in Gram-negative bacteria, FQs are thought to primarily enter the cell through hydrophilic porin channels and to a lesser extent through the hydrophobic lipid bilayer [68,69]. Thus, the more hydrophobic a compound is, the better it can penetrate the lipid bilayer, while the opposite is true for diffusion through hydrophilic porin channels. Porins are transmembrane proteins that form a β -barrel structure, creating a water-filled channel that allows the passive transport of hydrophilic compounds [70–72]. They are the most abundant proteins in the outer

membrane of Gram-negative bacteria, with various types existing. FQs are known to penetrate the outer membrane through the non-specific porin OmpF.

Since typical MIC values for QAC-based disinfectants are several mg/L, *i.e.* much higher concentrations than those assessed for enzyme inhibitors, it seems implausible that quaternary quinolones **1a-h** and **2a-d** inhibit bacterial growth by disruption of the bacterial cell membrane only. Based on the literature above, we expect the charged quaternary quinolones to cross the outer membrane *via* porins as hydrophilic compounds, and their moderate affinity for bacterial cell membranes [38–40] (which is due to lipophilicity and ionic interactions of quaternary ammonium structure as in QACs) results in superior antibacterial activity compared to ciprofloxacin against mature *P. aeruginosa* biofilms. The latter effect has been evidenced at concentration of 50 μ M that is approximately an order of magnitude higher than the assessed MIC values (2.72 μ M for ciprofloxacin hydrochloride and 6.25 μ M for compounds **1e** and **1g**).

3. Conclusions

A set of novel dimethyl quaternary ammonium FQs was designed, synthesized, and evaluated in terms of their antibacterial, cytotoxic, and physicochemical properties. Previously investigated quaternary hybrids of FQ and *Safirinium* dyes were evaluated concurrently. The majority of the obtained compounds were found to be active against selected ESKAPE Gram-positive and Gram-negative bacterial pathogens, *i.e.* *Staphylococcus aureus* and *Pseudomonas aeruginosa*. N^+ -dimethyl ciprofloxacin derivatives **1e** and **1g** exhibited activity with MIC values of 6.25 μ M against both tested strains, while ciprofloxacin hybrid **2d** exhibited slightly weaker potency (MIC = 25 μ M). Compound **1f**, that is N^+ -

dimethyl quaternary analogue of gatifloxacin, was selective towards *S. aureus* (MIC = 6.25 μM). Moreover, the active derivatives 1e-g and 2d turned out to be also effective against biofilm in pre- and post-exposure experiments with MBIC values of 5 (1f) and 10 (1e,g) μM against *S. aureus*, and 25 μM (1e and 1g) against *P. aeruginosa*. The decreased viability of the treated cells was evidenced. The most active compounds turned out to be selective for bacterial cells, as they showed very low cytotoxicity in experiments involving non-cancerous cells. Structure-activity relationship analysis revealed that lipophilic cyclopropyl substituent within N1 position of the FQ skeleton was crucial for maintaining pronounced antibacterial activity, while quaternization of the N7 terminal aliphatic diamine was not detrimental to biological potency. The above observation can be further supported with the results acquired using immobilized artificial membrane chromatography (IAM-HPLC), where the most active quaternary compounds proved phospholipophilicity indices CHI in the range of 11.7–18.23. These values were slightly lower or comparable to the index established for the reference drug, ciprofloxacin (19.7). These results are particularly compelling since the studied quaternary FQs lack the typical equilibrium-driven interconversion between ionized and uncharged species. Furthermore, the molecular docking studies suggest that all the synthesized molecules can inhibit bacterial type II topoisomerases and act at the active sites in the FQ-binding mode. The conducted studies provide insight into the structure-activity relationship of FQ-based antibacterial agents, and the described molecules may be a promising starting point for the rational development of new, highly effective and well-tolerated antimicrobial agents.

4. Experimental section

4.1. Materials and methods

Reagents for synthesis were obtained from Acros Organics, Sigma-Aldrich, Fluka Analytical, or Alfa Aesar and used without further purification. Acetonitrile HPLC grade for liquid chromatography, sodium phosphate dibasic dihydrate, and sodium phosphate monobasic monohydrate were purchased from Sigma-Aldrich. Ultrapure water was obtained with Millipore Direct-Q 3 UVWater Purification System (Millipore Corporation, Bedford, MA, USA) and used for buffer mobile phase preparation.

Analytical thin-layer chromatography (TLC) was performed on silica gel Merck 60 F254 plates (0.25 mm) with UV light visualization. The IR (KBr) spectra were recorded on Thermo Scientific Nicolet 380 FT-IR spectrometer using KBr pellets. The ^1H NMR and ^{13}C NMR spectra were obtained using Bruker Avance II HD 400 MHz spectrometer, BBFO 31P-15 N probe, internally referenced to DMSO- d_6 (2.5 and 39.7 ppm, respectively). Melting points were determined on an X-4 or Boetius 545 melting point apparatus with a microscope and were uncorrected. The mass spectra for the reaction progress monitoring were recorded on Shimadzu single quadrupole LCMS 2010 eV mass spectrometer (mobile phase 50% water, 50% ACN with 0.1% acetic acid) while the high-resolution mass spectroscopy analyses were performed using 6550 iFunnel Q-TOF spectrometer (Agilent Technologies) coupled with UHPLC system 1290 Infinity (Agilent Technologies); column ZORBAX Eclipse Plus C18, Rapid Resolution HD 2.1×100 mm, 1.8 μm ; mobile phase 97-0% water, 3-100% ACN, 0.1% acetic acid (gradient time 7 min). Elemental analysis was carried out using Vario El Cube CHNS, Elementar. All compounds are >95% pure by HPLC (see Fig. S24).

4.2. Synthetic procedures

Compounds 3, 4, 5a,b, 6a,b, and 7a-c were obtained according to the literature procedures and their spectral data were in accordance with these previously reported [44,45].

4.2.1. General procedure for the preparation of quaternary ammonium (fluoro)quinolones 1a-h

Methyl iodide (0.093 mL, 1.50 mmol) was added to a solution of the appropriate (fluoro)quinolone (0.30 mmol) in anhydrous dimethylformamide (3 mL) and triethylamine (0.050 mL, 0.36 mmol). Reaction progress was monitored with TLC (chloroform/methanol 9:1) and LC-MS (methanol/acetonitrile 1:1). After complete conversion of the starting material, the precipitated product was filtered off, then washed with dimethylformamide (2 x 1 mL) and acetone (1 mL) to yield desired products 1a-h. The compounds were recrystallized from methanol prior to characterization.

4-(6-Carboxy-8-ethyl-5-oxo-5,8-dihydropyrido[2,3-d]pyrimidin-2-yl)-1,1-dimethylpiperazin-1-ium iodide (1a)

Synthesized from 0.091 g of pipemidic acid. Yield: 57% (0.085 g); mp 296 °C with decomposition; IR (KBr): 3435, 3050, 3004, 2936, 1718, 1643, 1607, 1541, 1514, 1485, 1464, 1355, 1258, 951, 815, 716 cm^{-1} ; ^1H NMR (400 MHz, DMSO- d_6): δ = 1.38 (t, J = 7.1 Hz, 3H, CH₃), 3.25 (s, 6H, CH₃), 3.55–3.59 (m, 4H, CH₂), 4.27–4.31 (m, 4H, CH₂), 4.47 (q, J = 7.1 Hz, 2H, CH₂), 9.04 (s, 1H, CH), 9.32 (s, 1H, CH), 14.66 (bs, 1H, OH); ^{13}C NMR (100 MHz, DMSO- d_6): δ = 15.0, 38.4, 46.5, 51.1, 54.9, 109.9, 110.4, 151.5, 155.5, 161.0, 161.1, 165.6, 177.7; MS (ESI) m/z : 332 [M]⁺; Anal. calc. for C₁₆H₂₂N₅O₃ x 2H₂O: C 38.80, H 5.29, N 14.14, Found: C 38.67, H 5.41, N 13.94.

4-(6-Carboxy-8-ethyl-3-fluoro-5-oxo-5,8-dihydro-1,8-naphthyridin-2-yl)-1,1-dimethylpiperazin-1-ium iodide (1b)

Synthesized from 0.096 g of enoxacin. Yield: 41% (0.063 g); mp 263–265 °C; IR (KBr): 3435, 3057, 3004, 2971, 2933, 2858, 1713, 1632, 1480, 1463, 1269, 940, 808, 746 cm^{-1} ; ^1H NMR (400 MHz, DMSO- d_6): δ = 1.42 (t, J = 7.1 Hz, 3H, CH₃), 3.25 (s, 6H, CH₃), 3.59–3.61 (m, 4H, CH₂), 4.16–4.19 (m, 4H, CH₂), 4.56 (q, J = 7.1 Hz, 2H, CH₂), 8.25 (d, $^3J_{\text{FH}}$ = 13.2 Hz, 1H, CH), 9.05 (s, 1H, CH), 15.17 (bs, 1H, OH); ^{13}C NMR (100 MHz, DMSO- d_6): δ = 15.3, 41.2 (d, $^4J_{\text{CF}}$ = 8.8 Hz), 47.8, 51.3, 60.3, 108.7, 114.2 (d, $^3J_{\text{CF}}$ = 3.6 Hz), 120.6 (d, $^2J_{\text{CF}}$ = 22.0 Hz), 145.0, 147.5 (d, $^1J_{\text{CF}}$ = 259.0 Hz), 148.5, 150.0 (d, $^2J_{\text{CF}}$ = 9.5 Hz), 166.2, 176.9 (d, $^4J_{\text{CF}}$ = 2.2 Hz); MS (ESI) m/z : 349 [M]⁺; HRMS m/z : 349.1667 (anal.), 349.1670 (calcd. for C₁₇H₂₂FN₄O₃) [M]⁺; Anal. calc. for C₁₇H₂₂FN₄O₃ x 2H₂O: C 39.85, H 5.12, N 10.94, Found: C 39.72, H 5.40, N 11.09.

4-(3-Carboxy-1-ethyl-6-fluoro-4-oxo-1,4-dihydroquinolin-7-yl)-1,1-dimethylpiperazin-1-ium iodide (1c)

Synthesized from 0.096 g of 7a. Yield: 54% (0.083 g); mp 249–253 °C; IR (KBr): 3454, 3047, 3005, 2932, 2864, 1706, 1629, 1487, 1274, 1247, 938, 805, 752 cm^{-1} ; ^1H NMR (400 MHz, DMSO- d_6): δ = 1.47 (t, J = 7.2 Hz, 3H, CH₃), 3.27 (s, 6H, CH₃), 3.65–3.66 (m, 4H, CH₂), 3.72–3.73 (m, 4H, CH₂), 4.63 (q, J = 7.2 Hz, 2H, CH₂), 7.32 (d, $^4J_{\text{FH}}$ = 7.3 Hz, 1H, CH), 8.01 (d, $^3J_{\text{FH}}$ = 13.2 Hz, 1H, CH), 9.01 (s, 1H, CH), 15.25 (bs, 1H, OH); ^{13}C NMR (100 MHz, DMSO- d_6): δ = 15.0, 43.7 (d, $^4J_{\text{CF}}$ = 5.1 Hz), 49.7, 51.1, 60.5, 107.5 (d, $^3J_{\text{CF}}$ = 2.9 Hz), 107.7, 111.9 (d, $^2J_{\text{CF}}$ = 22.7 Hz), 120.6 (d, $^3J_{\text{CF}}$ = 7.3 Hz), 137.5, 144.3 (d, $^2J_{\text{CF}}$ = 10.2 Hz), 149.3, 153.1 (d, $^1J_{\text{CF}}$ = 249.4 Hz), 166.5, 176.9 (d, $^4J_{\text{CF}}$ = 2.2 Hz); MS (ESI) m/z : 348 [M]⁺; Anal. calc. for C₁₈H₂₃FIN₃O₃ x 2H₂O: C 42.28, H 5.32, N 8.22, Found: C 41.93, H 5.61, N 7.86.

4-(3-Carboxy-1-ethyl-6,8-difluoro-4-oxo-1,4-dihydroquinolin-7-yl)-1,1,2-trimethylpiperazin-1-ium iodide (1d)

Synthesized from 0.105 g of lomefloxacin. Yield: 50% (0.082 g); mp 265 °C with decomposition; IR (KBr): 3489, 2996, 2974, 2926, 1735, 1625, 1611, 1522, 1487, 1467, 1448, 1252, 1116, 1056, 804, 738 cm^{-1} ; ^1H NMR (400 MHz, DMSO- d_6): δ = 1.32 (d, J = 6.6 Hz, 3H, CH₃), 1.47 (t, J = 6.6 Hz, 3H, CH₃), 3.10 (s, 3H, CH₃), 3.23 (s, 3H, CH₃), 3.62–3.67 (m, 5H, 1xCH, 2xCH₂), 3.78–3.83 (m, 2H, CH₂), 4.61 (q, J = 6.6 Hz, 2H, CH₂), 7.95 (dd, $^3J_{\text{FH}}$ = 11.8 Hz, $^5J_{\text{FH}}$ = 1.8 Hz, 1H, CH), 8.98 (s, 1H, CH), 14.82 (bs, 1H, OH); ^{13}C NMR (100 MHz, DMSO- d_6): δ = 11.9, 16.5 (d, $^5J_{\text{CF}}$ = 5.1 Hz), 42.2, 44.8, 50.4 (d, $^4J_{\text{CF}}$ = 4.4 Hz), 53.1, 54.2 (d, $^4J_{\text{CF}}$ = 15.4 Hz), 63.2, 66.8, 107.6, 121.8 (d, $^2J_{\text{CF}}$ = 8.8 Hz), 127.6 (d, $^2J_{\text{CF}}$ = 7.4 Hz), 131.6 (d, $^3J_{\text{CF}}$ = 4.4 Hz), 132.5 (d, $^2J_{\text{CF}}$ = 13.9 Hz), 146.5 (d, $^1J_{\text{CF}}$ = 257.5 Hz), 151.9, 154.9 (d, $^1J_{\text{CF}}$ = 242.1 Hz), 165.9, 176.0 (d, $^4J_{\text{CF}}$ = 2.2 Hz); MS (ESI) m/z : 380 [M]⁺; HRMS m/z : 380.1774 (anal.),

380.1780 (calcd. for $C_{19}H_{24}F_2N_3O_3^+$) $[M]^+$; Anal. calc. for $C_{19}H_{24}F_2IN_3O_3 \times 2H_2O$: C 42.00, H 5.19, N 7.73, Found: C 41.77, H 5.32, N 7.54.

4-(3-Carboxy-1-cyclopropyl-6-fluoro-4-oxo-1,4-dihydroquinolin-7-yl)-1,1-dimethylpiperazin-1-ium iodide (**1e**)

Synthesized from 0.099 g of **7b**. Yield: 80% (0.125 g); mp 259–261 °C; IR (KBr): 3458, 3079, 3022, 2920, 1720, 1633, 1493, 1454, 1270, 942, 805, 748 cm^{-1} ; 1H NMR (400 MHz, DMSO- d_6): δ = 1.20–1.25 (m, 2H, CH₂), 1.33–1.36 (m, 2H, CH₂), 3.27 (s, 6H, CH₃), 3.66–3.67 (m, 4H, CH₂), 3.72–3.73 (m, 4H, CH₂), 4.81–4.83 (m, 1H, CH), 7.68 (d, $^4J_{FH}$ = 7.6 Hz, 1H, CH), 8.00 (d, $^3J_{FH}$ = 13.2 Hz, 1H, CH), 8.71 (s, 1H, CH), 15.11 (bs, 1H, OH); ^{13}C NMR (100 MHz, DMSO- d_6): δ = 8.2, 36.5, 43.6 (d, $^2J_{CF}$ = 5.1 Hz), 51.1, 60.6, 107.3, 107.9 (d, $^3J_{CF}$ = 3.0 Hz), 111.7 (d, $^2J_{CF}$ = 22.7 Hz), 120.1 (d, $^3J_{CF}$ = 8.1 Hz), 139.4, 144.0 (d, $^2J_{CF}$ = 10.3 Hz), 148.9, 153.3 (d, $^1J_{CF}$ = 249.4 Hz), 166.4, 176.9 (d, $^4J_{CF}$ = 3.0 Hz); MS (ESI) m/z : 360 $[M]^+$; Anal. calc. for $C_{19}H_{23}FIN_3O_3 \times 2H_2O$: C 43.61, H 5.20, N 8.03, Found: C 43.45, H 5.02, N 7.82.

4-(3-Carboxy-1-cyclopropyl-6-fluoro-8-methoxy-4-oxo-1,4-dihydroquinolin-7-yl)-1,1,2-trimethylpiperazin-1-ium iodide (**1f**)

Synthesized from 0.113 g of gatifloxacin. Yield: 52% (0.088 g); mp 227–229 °C; IR (KBr): 3436, 3066, 3005, 2858, 1721, 1619, 1517, 1458, 1313, 1059, 991, 807 cm^{-1} ; 1H NMR (400 MHz, DMSO- d_6): δ = 1.04–1.07 (m, 2H, CH₂), 1.13–1.15 (m, 2H, CH₂), 1.34 (d, J = 6.6 Hz, 3H, CH₃), 3.11 (s, 3H, CH₃), 3.26 (s, 3H, CH₃), 3.57–3.68 (m, 5H, 1xCH, 2xCH₂), 3.74–3.82 (m, 2H, CH₂), 3.84 (s, 3H, OCH₃), 4.17–4.21 (m, 1H, CH), 7.83 (d, $^3J_{FH}$ = 11.9 Hz, 1H, CH), 8.74 (s, 1H, CH), 14.84 (bs, 1H, OH); ^{13}C NMR (100 MHz, DMSO- d_6): δ = 9.5, 11.2, 41.2, 42.0, 44.7 (d, $^4J_{CF}$ = 3.7 Hz), 50.4 (d, $^4J_{CF}$ = 5.1 Hz), 53.2, 63.4, 63.7, 66.9, 107.1, 107.2 (d, $^2J_{CF}$ = 23.4 Hz), 122.3 (d, $^3J_{CF}$ = 8.8 Hz), 134.4 (d, $^4J_{CF}$ = 1.4 Hz), 137.8 (d, $^2J_{CF}$ = 11.7 Hz), 146.7 (d, $^3J_{CF}$ = 5.1 Hz), 151.3, 155.7 (d, $^1J_{CF}$ = 250.2 Hz), 166.0, 176.8 (d, $^4J_{CF}$ = 3.6 Hz); MS (ESI) m/z : 404 $[M]^+$; HRMS m/z : 404.1974 (anal.), 404.1980 (calcd. for $C_{21}H_{27}FN_3O_4^+$) $[M]^+$; Anal. calc. for $C_{21}H_{27}FIN_3O_4 \times 2H_2O$: C 44.45, H 5.51, N 7.41, Found: C 44.17, H 5.13, N 7.15.

4-(3-Carboxy-1-cyclopropyl-6-fluoro-4-oxo-1,4-dihydroquinolin-7-yl)-1,1-dimethyl-1,4-diazepan-1-ium iodide (**1g**)

Synthesized from 0.104 g of **7c**. Yield: 63% (0.101 g); mp 295 °C with decomposition; IR (KBr): 3437, 3076, 2995, 2924, 2854, 1716, 1630, 1509, 1477, 1408, 1382, 1269, 1247, 1188, 1080, 1037, 985, 825, 817, 803, 744 cm^{-1} ; 1H NMR (400 MHz, DMSO- d_6): δ = 1.18–1.22 (m, 2H, CH₂), 1.32–1.35 (m, 2H, CH₂), 2.33–2.36 (m, 2H, CH₂), 3.21 (s, 6H, CH₃), 3.59–3.66 (m, 4H, CH₂), 3.77–3.81 (m, 4H, CH₂), 3.88–3.91 (m, 1H, CH), 7.39 (d, $^4J_{FH}$ = 7.8 Hz, 1H, CH), 7.92 (d, $^3J_{FH}$ = 14.2 Hz, 1H, CH), 8.65 (s, 1H, CH), 15.29 (bs, 1H, OH); ^{13}C NMR (100 MHz, DMSO- d_6): δ = 8.1, 36.3, 44.8, 45.2, 49.5, 52.7, 64.1, 68.2, 104.1, 105.2 (d, $^2J_{CF}$ = 32.2 Hz), 106.9 (d, $^3J_{CF}$ = 4.4 Hz), 124.7 (d, $^3J_{CF}$ = 8.1 Hz), 130.5, 142.1 (d, $^2J_{CF}$ = 19.6 Hz), 147.1, 153.7 (d, $^1J_{CF}$ = 253.1 Hz), 166.6, 181.9; MS (ESI) m/z : 374 $[M]^+$; HRMS m/z : 374.1868 (anal.), 374.1874 (calcd. for $C_{20}H_{25}FN_3O_3^+$) $[M]^+$; Anal. calc. for $C_{20}H_{25}FIN_3O_3 \times 2H_2O$: C 44.70, H 5.44, N 7.82, Found: C 44.52, H 5.12, N 7.63.

6-(3-Carboxy-1-cyclopropyl-6-fluoro-8-methoxy-4-oxo-1,4-dihydroquinolin-7-yl)-1,1-dimethyloctahydro-1H-pyrrolo[3,4-b]pyridin-1-ium iodide (**1h**)

Synthesized from 0.120 g of moxifloxacin. Yield: 40% (0.072 g); mp 220–222 °C; IR (KBr): 3434, 3075, 3012, 2939, 2875, 1733, 1621, 1514, 1450, 1358, 1313, 1058, 803 cm^{-1} ; 1H NMR (400 MHz, DMSO- d_6): δ = 0.89–1.03 (m, 2H, CH₂), 1.13–1.25 (m, 2H, CH₂), 1.49–1.52 (m, 1H, CH₂), 1.80–1.87 (m, 2H, CH₂), 1.98–2.00 (m, 1H, CH₂), 2.82–2.89 (m, 1H, CH), 3.13 (s, 3H, CH₃), 3.29 (s, 3H, CH₃), 3.41–3.45 (m, 2H, CH₂), 3.63 (s, 3H, OCH₃), 3.66–3.72 (m, 2H, CH₂), 3.95–3.99 (m, 1H, CH), 4.14–4.19 (m, 1H, CH), 4.20–4.23 (m, 2H, CH₂), 7.75 (d, $^3J_{FH}$ = 13.7 Hz, 1H, CH), 8.70 (s, 1H, CH), 15.05 (bs, 1H, OH); ^{13}C NMR (100 MHz, DMSO- d_6): δ = 8.7, 10.2, 18.8, 22.1, 41.2, 52.3, 53.5, 54.9 (d, $^4J_{CF}$ = 8.1 Hz), 56.0 (d, $^4J_{CF}$ = 5.9 Hz), 57.5, 62.4, 68.5, 107.0, 107.0 (d, $^2J_{CF}$ = 23.4 Hz), 119.1 (d, $^3J_{CF}$ = 8.8 Hz), 134.8, 136.4 (d, $^2J_{CF}$ = 11.0 Hz), 142.8 (d, $^3J_{CF}$ = 7.4 Hz), 150.9, 153.8 (d, $^1J_{CF}$ = 249.5 Hz), 166.21,

176.6 (d, $^4J_{CF}$ = 2.9 Hz); MS (ESI) m/z : 430 $[M]^+$; HRMS m/z : 430.2130 (anal.), 430.2137 (calcd. for $C_{23}H_{29}FN_3O_4^+$) $[M]^+$; Anal. calc. for $C_{23}H_{29}FIN_3O_4 \times 2H_2O$: C 46.55, H 5.61, N 7.08, Found: C 46.19, H 5.93, N 6.79.

4.2.2. Synthesis of fluoroquinolone-Safirinium Q hybrids (**2a-d**)

Compounds **2a-c** were synthesized and reported by us earlier [38]. The hybrid compound **2d** was synthesized accordingly from fluoroquinolone (**g**), formaldehyde, and isoxazolo[3,4-*b*]pyridine-3 (1*H*)-one. The latter compound was synthesized in a multi-step procedure from aniline in accordance with the previously described synthetic route [73,74].

4-Carboxy-4'-(3-carboxy-1-cyclopropyl-6-fluoro-4-oxo-1,4-dihydroquinolin-7-yl)-1*H*-spiro[1,2,4]triazolo[4,3-*a*]quinoline-2,1'-[1,4]diazepan-1'-ium chloride (**2d**)

Isoxazolo[3,4-*b*]quinolin-3(1*H*)-one (0.050 g, 0.27 mmol), 35 wt% solution of formaldehyde (0.846 mL, 1.08 mmol) and 1-cyclopropyl-7-(1,4-diazepan-1-yl)-6-fluoro-4-oxo-1,4-dihydroquinoline-3-carboxylic acid (**g**, 0.093 g, 0.27 mmol) were dissolved in methanol (25 mL) and stirred at the room temperature. The progress of the reaction was monitored with TLC (chloroform/methanol 9:1) and LC-MS (methanol/acetonitrile 1:1). After 12 h the reaction mixture was evaporated under reduced pressure and the resultant solid was washed with acetone (3 x 3 mL). The crude product was recrystallized from methanol and the obtained pure compound was converted quantitatively into the hydrochloride form with HCl methanolic solution.

Yield: 75% (0.127 g); mp 199–201 °C; IR (KBr): 3408, 3019, 2926, 1713, 1625, 1572, 1508, 1460, 1216, 1169, 1066, 1028, 822, 786, 747 cm^{-1} ; 1H NMR (400 MHz, DMSO- d_6): δ = 1.18–1.22 (m, 2H, CH₂), 1.33–1.35 (m, 2H, CH₂), 2.40–2.46 (m, 2H, CH₂), 3.67–3.82 (m, 4H, CH₂), 4.04–4.06 (m, 2H, CH₂), 4.14–4.18 (m, 2H, CH₂), 4.31–4.35 (m, 1H, CH₂), 5.96–6.10 (m, 2H, CH₂), 7.24 (d, J = 7.9 Hz, 1H, CH), 7.38–7.44 (m, 2H, CH), 7.83 (t, J = 7.9 Hz, 1H, CH), 7.94 (d, $^3J_{FH}$ = 14.1 Hz, 1H, CH), 8.03 (d, J = 7.9 Hz, 1H, CH), 8.65 (s, 1H, CH), 8.76 (s, 1H, CH), 13.58 (bs, 1H, OH), 15.30 (bs, 1H, OH); ^{13}C NMR (100 MHz, DMSO- d_6): δ = 8.1, 21.4, 31.2, 36.3, 49.1, 66.7 (d, $^4J_{CF}$ = 1.5 Hz), 69.3 (d, $^4J_{CF}$ = 5.1 Hz), 75.9, 103.9 (d, $^3J_{CF}$ = 5.1 Hz), 106.9, 111.5 (d, $^2J_{CF}$ = 24.2 Hz), 114.7 (d, $^2J_{CF}$ = 11.7 Hz), 117.0, 120.3, 124.1, 131.6, 134.9, 136.3, 139.7, 144.7 (d, $^3J_{CF}$ = 10.3 Hz), 146.5, 148.2, 152.0 (d, $^1J_{CF}$ = 246.5 Hz), 152.9, 153.7 163.6, 166.5, 176.5; MS (ESI) m/z : 544 $[M]^+$; HRMS m/z : 544.1982 (anal.), 544.1991 (calcd. for $C_{29}H_{27}FN_5O_5^+$) $[M]^+$; Anal. calc. for $C_{29}H_{27}ClFN_5O_5 \times 3H_2O$: C 54.93, H 5.25, N 11.05, Found: C 54.68, H 5.53, N 10.72.

4.3. Crystal structure determination

The single-crystal X-ray diffraction data for compound **1e** were collected at 100(2) K using Oxford Diffraction Xcalibur CCD diffractometer with the graphite-monochromated MoK α radiation (λ = 0.7107 Å). The CrysAlisPro 1.171.39.27b program was used for data collection, cell refinement, and data reduction [75]. The intensities were corrected for Lorentz and polarization effects. A multi-scan absorption correction was applied. The structure was solved using the direct methods implemented in the SHELXT [76] and refined with the SHELXL-18/3 program [77], both operating under WinGX [78]. All non-H atoms were refined with anisotropic displacement parameters. The hydrogen atoms attached to carboxyl and water oxygen atoms were found in the difference Fourier maps and not refined. All remaining ones were positioned geometrically and refined using the riding model with $U_{iso}(H)$ = 1.2U_{eq} (CH and CH₂) or $U_{iso}(H)$ = 1.5U_{eq} (CH₃).

The cif file for **1e** was deposited at the Cambridge Crystallographic Data Centre [79] as a supplementary material (CCDC 2195742). Copy of the data can be obtained free of charge on application to CCDC, 12 Union Road, Cambridge CB21EZ, UK (Fax: +44 1223-336-033; e-mail: deposit@ccdc.cam.ac.uk or [www: http://www.ccdc.cam.ac.uk/contents/retrieving.html](http://www.ccdc.cam.ac.uk/contents/retrieving.html)).

Crystal data for **1e** ($C_{19}H_{27}N_3O_5FI$, $M = 523.33 \text{ g mol}^{-1}$): monoclinic, space group $P2_1/c$, $a = 16.8706(12) \text{ \AA}$, $b = 6.9331(4) \text{ \AA}$, $c = 17.7532(9) \text{ \AA}$, $\beta = 93.530(6)^\circ$, $V = 2072.6(2) \text{ \AA}^3$, $Z = 4$, $\mu = 1.590 \text{ mm}^{-1}$, $D_{\text{calc}} = 1.677 \text{ g cm}^{-3}$, 10575 reflections measured ($2.53 \leq \theta \leq 27.482^\circ$), 4734 unique ($R_{\text{int}} = 0.045$) which were used in all calculations. The final $R_1 = 0.0479$ ($I > 2\sigma(I)$) and $wR_2 = 0.1270$ (all data), $\text{GOF} = 1.026$ and $\rho_{\text{min./max.}} = -0.72/1.39 \text{ e \AA}^{-3}$

4.4. HPLC

4.4.1. Analytes

The analytical standards of octanonophenone, butyrophenone, and acetanilidine were provided by Alfa Aesar (Haverhill, MA, USA); acetaminophen, theophylline, benzimidazole, acetophenone, and indole were purchased from Sigma-Aldrich (Steinheim, Germany); heptanophenone, hexanophenone, valerophenone, propiophenone, acetophenone were bought from Acros Organic (Massachusetts, United States). All the compounds listed above were used as model substances in order to determine CHI indices of the studied **1a-h** and **2a-d** derivatives according to the protocol proposed by Valko and co-workers [52]. All studied compounds were dissolved in DMSO to obtain a concentration of 1 mg/mL and stored at 2–8 °C prior to analyses.

4.4.2. IAM-HPLC

All HPLC experiments were carried out using a Prominence-1 LC-2030C 3D HPLC system (Shimadzu, Japan) equipped with a DAD detector and controlled by the LabSolution system (version 5.90 Shimadzu, Japan). The stock solutions of solutes were diluted to obtain concentrations of 100 µg/mL, and the injected volume was 5 µL. The IAM-HPLC analyses were carried out on IAM.PC.DD2 column (10 × 4.6 mm; particle size 10.0 µm with IAM guard column; Regis Technologies, USA) with a linear gradient 0–85% phase B (where phase A was 10 mM phosphoric buffer at pH 7.4 and phase B was acetonitrile) at a flow rate of 1.5 mL/min. The temperature of the chromatographic column was controlled and set to 30.0 °C and the analysis time was 6.5 min. Each HPLC analysis was run in duplicate.

4.5. Biological activity

4.5.1. Determination of antibacterial activity

Bacterial strains *P. aeruginosa* ATCC 27853 and *S. aureus* ATCC 29213 purchased from Micro-biologics Inc. (St. Cloud, MN, USA) were used as representative of Gram-negative and Gram-positive human pathogens for the screening and MIC determinations of all compounds. Both assays were performed by the broth microdilution method in 96-well plate format according to the Clinical and Laboratory Standards Institute (CLSI) guidelines [80]. Bacterial colonies were taken from the Mueller Hinton agar (MHA, Neogen) overnight culture, inoculated into 0.9% saline solution, and vortexed to ensure that the bacterial suspension was homogeneous. Bacterial suspensions were analyzed using a densitometer (DEN-1, BioSan, Warren MI, USA) and adjusted to 1×10^6 CFU/mL by diluting with cation-adjusted Mueller Hinton broth (CAMHB, BD). An equal volume of bacterial suspension and test compound solution were mixed together into plate wells (Thermo Fisher Scientific) and incubated for 24 h at 37 °C. Absorbance values measured at 600 nm using MultiskanGO plate reader (Thermo Fisher Scientific, Vantaa, Finland) were used for evaluating the antibacterial effects, by comparing them to untreated controls, and expressed as a percentage of growth inhibition. Biomek i7 automated liquid handling workstation (Beckman Coulter) was used for the assay plate preparation with exception of the addition of bacterial suspension, which was done manually. In the screening assays, compounds were tested at 50 µM. If the compound led to $\geq 80\%$ (\pm SD) of bacterial growth inhibition, MIC determinations were performed. MIC assays were conducted with compound concentrations ranging from 75 to 0.78 µM. MIC was defined as the lowest compound concentration at which bacterial growth was

inhibited by $\geq 90\%$ compared to compound-free control. Visual assessment was also performed to confirm the results from the plate reader. Ciprofloxacin hydrochloride (ICN Biomedicals) at 2.72 µM and 1.36 µM were used as positive controls for *P. aeruginosa* and *S. aureus*, respectively in all assays. Two independent experiments with three technical replicates each were performed.

4.5.2. Determination of antibiofilm activity

Two strains of bacteria were used, *S. aureus* ATCC 25923 and *P. aeruginosa* ATCC 15442 (ATCC; Wesel, Germany). Bacteria were grown overnight on tryptic soy agar (TSA, Lab M Ltd) plates at 37 °C for 16–18 h. New colonies were inoculated on 5 mL fresh tryptic soy broth (TSB, Lab M Ltd) and incubated at 37 °C and 220 rpm for about 2.5–3 h to obtain a culture with an optical density (OD) of 0.3–0.35. The grown culture was diluted 100 times in TSB to reach a concentration of approximately 10^6 CFU/mL.

The antibiofilm activity was evaluated by means of pre- and post-exposure experiments, where one biological test was performed with two technical replicates for each condition. For pre-exposure experiments, 4 µL of the tested compound or ciprofloxacin used as a control at a defined concentration (50x stock in DMSO) and 196 µL of the diluted bacterial culture were added per well of sterile 96-microwell flat-bottom plates (Thermo Fisher Scientific, Nunclon Delta Surface). A negative control applied for biofilm formation was 200 µL of bacterial suspension without the tested substance. The plates were incubated on a plate shaker at 220 rpm for 18 h at a temperature of 37 °C.

For post-exposure experiments, 200 µL of diluted bacterial culture was added per well of a sterile 96-microwell plate to all test wells. The plate was incubated for 18 h at 37 °C on a plate shaker at 220 rpm. Afterwards, the planktonic solution was removed with caution without touching the newly grown biofilm, using a multichannel pipette. Next, 4 µL of a test compound or control antibiotic (50x stock in DMSO) and 196 µL of sterile TSB were added. The plates were again incubated at 37 °C on a plate shaker at 220 rpm for an extra 24 h [54]. The negative (wells containing untreated bacteria) and blank controls (wells containing only TSB) were present in all plates.

After the incubation, several experimental procedures were applied to evaluate the growth and viability of planktonic (free-floating) bacteria as well as the viability and total biomass of the biofilms.

To evaluate the growth of planktonic bacteria, 190 µL of well content was transferred very carefully avoiding creating any air bubbles to a clean plate using a multichannel pipette. The optical density was measured at 595 nm using a Varioskan LUX Multimode Plate Reader (Thermo Fisher Scientific, Vantaa, Finland).

Next, the viability of planktonic cells was measured by adding 10 µL of resazurin (stock solution 20 mM or 200 µM, Sigma-Aldrich, St. Louis, MO, USA) and mixed by pipetting. The plate was incubated at 37 °C in darkness on the plate shaker at 200 rpm for 4–10 min depending on the bacteria strain that was tested. The fluorescence was measured at $\lambda_{\text{excitation}} = 560 \text{ nm}$ and $\lambda_{\text{emission}} = 590 \text{ nm}$ using the Varioskan LUX Multimode Plate Reader.

To measure the metabolic activity of the cells and the total biomass of the biofilms, resazurin and crystal violet assays were used, respectively. Firstly, biofilms were prepared for the resazurin staining by once carefully washing with 200 µL of phosphate-buffered saline (PBS, Thermo Fisher Scientific Oxoid Ltd, Basingstoke, England) to avoid harming the biofilms. Subsequently, the biofilms were stained by adding 200 µL of a resazurin diluted solution (1:20 in PBS) per well. The plates were incubated at 37 °C in darkness on a plate shaker 200 rpm for approximately 30 min and 1 h while staining the *S. aureus* and *P. aeruginosa*, respectively, then the fluorescence was measured as described above.

Afterwards, the resazurin solution was removed and the biofilms were fixed by adding 200 µL of ethanol per well. The plate was then incubated for 15 min at room temperature (RT) without shaking. After that time, the ethanol was carefully removed and the wells were left to

dry completely. The biofilms were stained with crystal violet (190 μL , 100x dilution of commercial stock, Sigma-Aldrich, St. Louis, MO, USA) for 5 min (RT), without shaking and then washed twice with Milli-Q-water. The remaining dye was then solubilized in 96% ethanol (200 μL per well) and incubated again at RT for about 1 h. The absorbance was measured at 595 nm using a Multiskan Sky (Thermo Fisher Scientific, Vantaa, Finland) [55,56].

Then, the number of viable cells within the biofilm was evaluated from the same wells by CFU counting. After washing once with PBS, 100 μL of PBS was added to each well and the bottom of the wells was scraped to detach the formed biofilm. Serial 10-fold dilutions were made in PBS and 10 μL of appropriate solutions were placed on agar plates. The plates were incubated for 24 h and the grown colonies of bacteria were counted for those spots where 3–30 colonies were observed.

4.5.3. *In vitro* cytotoxicity assays

Gibco™ (Thermo Fisher Scientific, Massachusetts, USA) reagents were used for cell culturing. Mouse embryonic fibroblast Balb 3T3 clone A31 cell line (ECACC 86110401) was maintained in GlutaMAX high glucose Dulbecco's Modified Eagle's Medium (DMEM, Gibco) with 5% (v/v) of Newborn Calf Serum (NBCS), 5% (v/v) Fetal Bovine Serum (FBS), and 100 units/mL penicillin and streptomycin at +37 °C and 5% CO₂. One day before the compound exposure, cells were seeded into a white-frame, clear-bottom polystyrene 96-well microplate (PerkinElmer) at the density of 6 000 cells/well in 200 μL of cell culture medium. The cells were grown at 37 °C, 5% CO₂ until they reached 70–80% confluence (approximately 20–24 h). Stock solutions of test compounds and positive control (camptothecin, Sigma-Aldrich, Saint Louis, MO, USA) were prepared in DMSO and diluted into assay medium (growth medium with 2.5% NBCS and 2.5% FBS) to the final concentration. The final DMSO concentration was 0.5% in all samples. The culture medium was removed from the plate and compounds in the assay medium were added, 200 μL /well. After 48 h incubation, the amount of ATP, which is directly proportional to the number of cells present in the culture, was quantified using CellTiter-Glo® Luminescent Cell Viability kit (Promega, Madison, WI, USA) according to the manufacturer's instructions with minor modifications. In brief, the assay medium was removed and the wells were washed with 100 μL of PBS, then 50 μL of fresh assay medium and 50 μL of the CellTiter-Glo® Reagent were added per well and mixed. The luminescence signal was measured by Varioskan LUX (Thermo Fisher Scientific) after 2 min of shaking and 10 min incubation at RT. The percentage of viability was calculated as follows: $(L_{\text{sample}} - L_{\text{blank control}})/(L_{\text{negative control}} - L_{\text{blank control}})$, where L is the average intensity of luminescence obtained in three technical replicates, the sample is the tested compound at a certain concentration, blank control is the medium with 0.5% DMSO and without cells, and negative control is the medium with 0.5% DMSO and cells. The CC₅₀ values were determined using logarithmic interpolation from 2 points flanking the threshold of 50% with the use of Excel 2016 software. The given values are the mean of two independent experiments \pm SD.

4.6. Computational studies

4.6.1. ADME/Tox calculation

SwissADME data were obtained using a web-based application available online [81]. As input canonical SMILES were used, next the calculated pharmacokinetic properties were downloaded as.csv data files and summarized in supplementary materials.

4.6.2. Ligand and protein preparation for modeling

The proteins were prepared using MAKE RECEPTOR software [65, 82,83]. The pocket around the ligand bound in the crystal structure was generated automatically and was not adjusted, which resulted in grid box sizes of 4645 and 4522 Å for *S. aureus* DNA gyrase and *S. pneumoniae* topoisomerase IV, respectively. Slow and effective “Molecular” method was used for “Cavity detection”, that is detection of binding sites. Outer

and inner contours of the grid box were calculated automatically as well with the use of “Balanced” settings for “Site Shape Potential” calculation, which once more resulted in different outer contour sizes depending on the bound ligand, 1423 and 1846 Å for *S. aureus* DNA gyrase and *S. pneumoniae* topoisomerase IV, respectively. The inner contours were disabled. As constraints for docking calculations, magnesium ions and Ser84 (*S. pneumoniae* ParC) were used.

The structures of compounds were prepared in SMILES notation taking account the chirality and appropriate protonation states. A library of conformers was generated with OMEGA default settings, which resulted in a maximum of 200 conformers per ligand [84,85].

4.6.3. Molecular docking

The compounds were docked using HYBRID algorithm [82,83]. Docking resolution was set to high; other settings were set as default. Ten docking solutions were inspected visually and the best ranked HYBRID-calculated conformations were used for analysis and representation. The docking protocols have been validated by re-docking the co-crystallized ligands with the RMSD values of 0.374 and 0.914 Å for 3rae and 5cdq, respectively.

Author contributions

JF designed the study and wrote the manuscript with support from KC, CDC, LM, and JS. JF and MM synthesized and characterized all the molecules reported with support from LM and JS. KC evaluated lipophilicity of the compounds. JF tested the antibacterial activity of the compounds and interpreted the results supervised by CDC and PT. MM and SGG designed and performed antibiofilm experiments supervised by KS and AF. JF carried out the cytotoxicity experiments supervised by HM and PI. JF performed docking experiments. All authors discussed the results and commented on the manuscript.

Funding

This work was supported by the Polish National Agency for Academic Exchange [grant number PPN/BEK/2019/1/00217]; the Academy of Finland (grant no. 321551), and Medical University of Gdańsk (Poland) subsidies. We thank OpenEye Scientific Software, Santa Fe, NM., for free academic licenses for the use of their software, and the DDCB core facility supported by the University of Helsinki (HiLIFE) and Biocenter Finland for access to bioactivity screening facilities.

Declaration of competing interest

The authors declare the following financial interests/personal relationships which may be considered as potential competing interests: Joanna Fedorowicz reports financial support was provided by Polish National Agency for Academic Exchange. Paivi Tammela reports financial support was provided by Academy of Finland. Joanna Fedorowicz reports financial support was provided by Medical University of Gdansk. Jaroslaw Saczewski reports equipment, drugs, or supplies was provided by OpenEye Scientific Software. Paivi Tammela reports equipment, drugs, or supplies was provided by University of Helsinki.

Data availability

Data will be made available on request.

Appendix A. Supplementary data

Supplementary data to this article can be found online at <https://doi.org/10.1016/j.ejmech.2023.115373>.

References

- [1] C.J. Murray, K.S. Ikuta, F. Sharara, L. Swetschinski, G. Robles Aguilar, A. Gray, et al., Global burden of bacterial antimicrobial resistance in 2019: a systematic analysis, *Lancet* 399 (2022) 629–655, [https://doi.org/10.1016/S0140-6736\(21\)02724-0](https://doi.org/10.1016/S0140-6736(21)02724-0).
- [2] D.I. Andersson, N.Q. Balaban, F. Baquero, P. Courvalin, P. Glaser, U. Gophna, R. Kishony, S. Molin, T. Tønjum, Antibiotic resistance: turning evolutionary principles into clinical reality, *FEMS Microbiol. Rev.* 44 (2021), <https://doi.org/10.1093/FEMSRE/FUAA001>. FUA001.
- [3] N.D. Friedman, E. Temkin, Y. Carmeli, The negative impact of antibiotic resistance, *MCI* 22 (2016) 416–422, <https://doi.org/10.1016/j.cmi.2015.12.002>.
- [4] Y. Zhu, W.E. Huang, Q. Yang, Clinical perspective of antimicrobial resistance in bacteria, *Infect. Drug Resist.* 15 (2022) 735–746, <https://doi.org/10.2147/IDR.S345574>.
- [5] R.C. Founou, L.L. Founou, S.Y. Essack, Clinical and economic impact of antibiotic resistance in developing countries: a systematic review and meta-analysis, *PLoS One* 12 (2017), e0189621, <https://doi.org/10.1371/journal.pone.0189621>.
- [6] S. Zaman, M. Hussain, R. Nye, V. Mehta, K.T. Mamun, N. Hossain, A review on antibiotic resistance: alarm bells are ringing, *Cureus* 9 (2017) e1403, <https://doi.org/10.7759/cureus.1403>.
- [7] C. Deng, H. Yan, J. Wang, K. Liu, B.-s. Liu, Y.-m. Shi, 1,2,3-Triazole-containing hybrids with potential antibacterial activity against ESKAPE pathogens, *Eur. J. Med. Chem.* 244 (2022), 114888, <https://doi.org/10.1016/j.ejmech.2022.114888>.
- [8] M. Durcik, A. Nyerges, Z. Skok, D. Gramec Skledar, J. Trontelj, N. Zidar, J. Ilaš, A. Zega, C.D. Cruz, P. Tammela, M. Welin, Y.R. Kimbung, D. Focht, O. Benek, T. Revesz, G. Draskovits, P.E. Szili, L. Daruka, C. Pal, D. Kikelj, L. Petrlin Masić, T. Tomasić, New dual ATP-competitive inhibitors of bacterial DNA gyrase and topoisomerase IV active against ESKAPE pathogens, *Eur. J. Med. Chem.* 213 (2021), 113200, <https://doi.org/10.1021/acs.jmedchem.2c01597>.
- [9] Q. Kong, Y. Yang, Recent advances in antibacterial agents, *Bioorg. Med. Chem. Lett.* 35 (2021), 127799, <https://doi.org/10.1016/j.bmcl.2021.127799>.
- [10] H. Liu, S.G. Mulholland, Appropriate antibiotic treatment of genitourinary infections in hospitalized patients, *Am. J. Med.* 118 (2005) 14–20, <https://doi.org/10.1016/j.amjmed.2005.05.009>.
- [11] Guidelines for the management of adults with hospital-acquired, ventilator-associated, and healthcare-associated pneumonia, *Am. J. Respir. Crit. Care Med.* 171 (2005) 388–416, <https://doi.org/10.1164/rccm.200405-644ST>.
- [12] Y. Jia, L. Zhao, The antibacterial activity of fluoroquinolone derivatives: an update (2018–2021), *Eur. J. Med. Chem.* 224 (2021), 113741, <https://doi.org/10.1016/j.ejmech.2021.113741>.
- [13] V. Sharma, R. Das, D.K.M.S. Gupta, K.N. Venugopala, R. Mailavaram, A.B. Nair, A. K. Shakya, P.K. Deb, Recent insight into the biological activities and SAR of quinolone derivatives as multifunctional scaffold, *Bioorg. Med. Chem.* 59 (2022), 116674, <https://doi.org/10.1016/j.bmc.2022.116674>.
- [14] M.I. Andersson, A.P. MacGowan, Development of the quinolones, *J. Antimicrob. Chemother.* 51 (2003) 1–11, <https://doi.org/10.1093/jac/dkg212>.
- [15] L. Feng, K. Lv, M. Liu, S. Wang, J. Zhao, X. You, S. Li, J. Cao, H. Guo, Synthesis and in vitro antibacterial activity of gemifloxacin derivatives containing a substituted benzyloxime moiety, *Eur. J. Med. Chem.* 55 (2012) 125–136, <https://doi.org/10.1016/j.ejmech.2012.07.010>.
- [16] S. Bhawsar, R. Kale, P. Deshpande, R. Yeole, S. Bhagwat, M. Patel, Design and synthesis of an oral prodrug alalevonadifloxacin for the treatment of MRSA infection, *Bioorg. Med. Chem. Lett.* 54 (2021), 128432, <https://doi.org/10.1016/j.bmcl.2021.128432>.
- [17] E. Pestova, J.J. Millichap, G.A. Noskin, L.R. Peterson, Intracellular targets of moxifloxacin: a comparison with other fluoroquinolones, *J. Antimicrob. Chemother.* 45 (2000) 583–590, <https://doi.org/10.1093/jac/45.5.583>.
- [18] R. Beyer, E. Pestova, J.J. Millichap, V. Stosor, G.A. Noskin, L.R.A. Peterson, Convenient assay for estimating the possible involvement of efflux of fluoroquinolones by streptococcus pneumoniae and staphylococcus aureus: evidence for diminished moxifloxacin, sparfloxacin, and trovafloxacin efflux, *Antimicrob. Agents Chemother.* 44 (2000) 798–801, <https://doi.org/10.1128/AAC.44.3.798-801.2000>.
- [19] T.A. Davies, L.M. Kelly, G.A. Pankuch, K.L. Credito, M.R. Jacobs, P.C. Appelbaum, Antipneumococcal activities of gemifloxacin compared to those of nine other agents, *Antimicrob. Agents Chemother.* 44 (2000) 304–310, <https://doi.org/10.1128/AAC.44.2.304-310.2000>.
- [20] S.V. Blokhina, A.V. Sharapova, M.V. Ol'khovich, T.V. Volkova, G.L. Perlovich, Solubility, lipophilicity and membrane permeability of some fluoroquinolone antimicrobials, *Eur. J. Pharmaceut. Sci.* 93 (2016) 29–37, <https://doi.org/10.1016/j.ejps.2016.07.016>.
- [21] G.E.-D.A.A. Abuo-Rahma, H.A. Sarhan, G.F.M. Gad, Design, synthesis, antibacterial activity and physicochemical parameters of novel N-4-piperazinyl derivatives of norfloxacin, *Bioorg. Med. Chem.* 17 (2009) 3879–3886, <https://doi.org/10.1016/j.bmc.2009.04.027>.
- [22] J.S. Chapman, N.H. Georgopadkou, Routes of quinolone permeation in *Escherichia coli*, *Antimicrob. Agents Chemother.* 32 (1988) 438–442, <https://doi.org/10.1128/AAC.32.4.438>.
- [23] A.J.H. Marshall, L.J.V. Piddock, Interaction of divalent cations, quinolones and bacteria, *J. Antimicrob. Chemother.* 34 (1994) 465–483, <https://doi.org/10.1093/jac/34.4.465>.
- [24] M.-H. Langlois, M. Montagu, J.-P. Dubost, J. Grellet, M.-C. Saux, Protonation equilibrium and lipophilicity of moxifloxacin, *J. Pharm. Biomed. Anal.* 37 (2005) 389–393, <https://doi.org/10.1016/j.jpba.2004.10.022>.
- [25] E.Y.W. Ng, M. Trucksis, D.C. Hooper, Quinolone resistance mediated by norA: physiologic characterization and relationship to flqB, a quinolone resistance locus on the staphylococcus aureus chromosome, *Antimicrob. Agents Chemother.* 38 (1994) 1345–1355, <https://doi.org/10.1128/AAC.38.6.1345>.
- [26] H. Nikaïdo, D.G. Thanassi, Penetration of lipophilic agents with multiple protonation sites into bacterial cells: tetracyclines and fluoroquinolones as examples, *Antimicrob. Agents Chemother.* 37 (1993) 1393–1399, <https://doi.org/10.1128/AAC.37.7.1393>.
- [27] J. Fedorowicz, J. Sączewski, Modifications of quinolones and fluoroquinolones: hybrid compounds and dual-action molecules, *Monatsh. Chem.* 149 (2018) 1199–1245, <https://doi.org/10.1007/s00706-018-2215-x>.
- [28] Y.-M. Tan, D. Li, F.-F. Li, M.F. Ansari, B. Fang, C.-H. Zhou, Pyrimidine-conjugated fluoroquinolones as new potential broad-spectrum antibacterial agents, *Bioorg. Med. Chem. Lett.* 73 (2022), 128885, <https://doi.org/10.1016/j.bmcl.2022.128885>.
- [29] J. Peek, B. Koirala, S.F. Brady, Synthesis and evaluation of dual-action kanglemycin-fluoroquinolone hybrid antibiotics, *Bioorg. Med. Chem. Lett.* 57 (2022), 128484, <https://doi.org/10.1016/j.bmcl.2021.128484>.
- [30] N.M. Ibrahim, S.H. Fahim, M. Hassan, A.E. Farag, H.H. Georgey, Design and synthesis of ciprofloxacin-sulfonamide hybrids to manipulate ciprofloxacin pharmacological qualities: potency and side effects, *Eur. J. Med. Chem.* 228 (2022), 114021, <https://doi.org/10.1016/j.ejmech.2021.114021>.
- [31] M. Samir, M. Ramadan, M.H. Abdelrahman, M.A.I. Elbastawesy, H.M. Halby, M. Abdel-Aziz, G.E.-D.A. Abuo-Rahma, New potent ciprofloxacin-uracil conjugates as DNA gyrase and topoisomerase IV inhibitors against methicillin-resistant *Staphylococcus aureus*, *Bioorg. Med. Chem.* 73 (2022), 117004, <https://doi.org/10.1016/j.bmc.2022.117004>.
- [32] B. Fois, Z. Skok, T. Tomasić, J. Ilaš, N. Zidar, A. Zega, L. Petrlin Masić, P. Szili, G. Draskovits, A.J. Nyerges, C. Pal, D. Kikelj, Dual *Escherichia coli* DNA gyrase A and B inhibitors with antibacterial activity, *ChemMedChem* 15 (2020) 265–269, <https://doi.org/10.1002/cmdc.202001534>.
- [33] W. Dan, J. Gao, X. Qi, J. Wang, J. Dai, Antibacterial quaternary ammonium agents: chemical diversity and biological mechanism, *Eur. J. Med. Chem.* 243 (2022), 114765, <https://doi.org/10.1016/j.ejmech.2022.114765>.
- [34] X. Xia, Y. Chen, L. Wang, Z.-G. Yang, X.-D. Ma, Z.-G. Zhao, H.-J. Yang, Synthesis of diosgenyl quaternary ammonium derivatives and their antitumor activity, *Steroids* 166 (2021), <https://doi.org/10.1016/j.steroids.2020.108774>.
- [35] M.M. Elbadawi, W.M. Eldehna, A.A. Abd El-Hafeez, W.R. Somaa, A. Albohy, S. T. Al-Rashood, K.K. Agama, E.B. Elkaeed, P. Ghosh, Y. Pommier, M. Abe, 2-arylquinolines as novel anticancer agents with dual EGFR/FAK kinase inhibitory activity: synthesis, biological evaluation, and molecular modelling insights, *J. Enzym. Inhib. Med. Chem.* 37 (2022) 349–372, <https://doi.org/10.1080/14756366.2021.2015344>.
- [36] C. Saturnino, A. Caruso, D. Iacopetta, C. Rosano, J. Ceramella, N. Muià, A. Mariconda, M.G. Bonomo, M. Ponassi, G. Rosace, M.S. Sincropi, P. Longo, Inhibition of human topoisomerase II by N,N,N-trimethylethanammonium iodide alkylcarbazole derivatives, *ChemMedChem* 13 (2018) 2635–2643, <https://doi.org/10.1002/cmdc.201800546>.
- [37] E. Sadowski, B. Bercot, A. Chauffour, C. Gomez, E. Varon, M. Mainardis, W. Sougakoff, C. Mayer, E. Sachon, G. Anquetin, A. Aubry, Lipophilic quinolone derivatives: synthesis and in vitro antibacterial evaluation, *Bioorg. Med. Chem. Lett.* 55 (2022), 128450, <https://doi.org/10.1016/j.bmcl.2021.128450>.
- [38] J. Fedorowicz, J. Sączewski, A. Konopacka, K. Waleron, D. Lejnowski, K. Ciura, T. Tomasić, Z. Skok, K. Savijoki, M. Morawska, S. Gilbert-Girard, A. Fallarero, Synthesis and biological evaluation of hybrid quinolone-based quaternary ammonium antibacterial agents, *Eur. J. Med. Chem.* 179 (2019) 576–590, <https://doi.org/10.1016/j.ejmech.2019.06.071>.
- [39] K. Ciura, J. Fedorowicz, F. Andrić, K.E. Greber, A. Gurgielewicz, W. Sawicki, J. Sączewski, Lipophilicity determination of quaternary (Fluoro)Quinolones by chromatographic and theoretical approaches, *Int. J. Mol. Sci.* 20 (2019) 5288, <https://doi.org/10.3390/ijms20215288>.
- [40] K. Ciura, J. Fedorowicz, H. Kapica, A. Adamkowska, W. Sawicki, J. Sączewski, Affinity of fluoroquinolone-safirinium dye hybrids to phospholipids estimated by IAM-HPLC, *Processes* 8 (2020) 1148, <https://doi.org/10.3390/pr8091148>.
- [41] M.J. Nieto, A.B. Pierini, N. Singh, C.R. McCurdy, R.H. Manzo, M.R. Mazzierie, SAR analysis of new dual targeting fluoroquinolones: implications of the benzenesulfonyl group, *Med. Chem.* 8 (2012) 349–360, <https://doi.org/10.2174/157340612800786633>.
- [42] M. F. Grill, R.K. Maganti, Neurotoxic effects associated with antibiotic use: management considerations, *Br. J. Clin. Pharmacol.* 72 (2011) 381–393, <https://doi.org/10.1111/j.1365-2125.2011.03991.x>.
- [43] X.-H. Li, Z.-L. Zhu, X.-L. Cheng, X.-D. Yang, Quantitative structure-pharmacokinetic/pharmacodynamic relationship for fluoroquinolones, *Pharm. Chem. J.* 41 (2007) 82–87, <https://doi.org/10.1007/s11094-007-0018-1>.
- [44] M.D. Wallace, N.F. Waraich, A.W. Debowski, M.G. Corral, A. Maxwell, J.S. Mynle, K.A. Stubbs, Developing ciprofloxacin analogues against plant DNA gyrase: a novel herbicide mode of action, *Chem* 54 (2018) 1869–1872, <https://doi.org/10.1039/c7cc09518j>.
- [45] H. Koga, A. Itoh, S. Murayama, S. Suzue, T. Irikura, Structure-activity relationships of antibacterial 6, 7-and 7, 8-disubstituted 1-alkyl-1, 4-dihydro-4-oxoquinoline-3-carboxylic acids, *J. Med. Chem.* 23 (1980) 1358–1363, <https://doi.org/10.1021/jm00186a014>.
- [46] J. Ali, P. Camilleri, M.B. Brown, A.J. Hutt, S.B. Kirton, Revisiting the general solubility equation: in silico prediction of aqueous solubility incorporating the effect of topographical polar surface area, *J. Chem. Inf. Model.* 52 (2012) 420–428, <https://doi.org/10.1021/ci200387c>.

- [47] C. Scavone, A. Mascolo, R. Ruggiero, L. Sportiello, C. Rafaniello, L. Berrino, A. Capuano, Quinolones-induced musculoskeletal, neurological, and psychiatric ADRs: a pharmacovigilance study based on data from the Italian spontaneous reporting system, *Front. Pharmacol.* 11 (2020) 428, <https://doi.org/10.3389/fphar.2020.00428>.
- [48] W.J. Egan, K.M. Merz, J.J. Baldwin, Prediction of drug absorption using multivariate statistics, *J. Med. Chem.* 43 (2000) 3867–3877, <https://doi.org/10.1021/jm000292e>.
- [49] A.K. Ghose, V.N. Viswanadhan, J.J. Wendoloski, A knowledge-based approach in designing combinatorial or medicinal chemistry libraries for drug discovery. 1. A qualitative and quantitative characterization of known drug databases, *J. Comb. Chem.* 1 (1999) 55–68, <https://doi.org/10.1021/cc9800071>.
- [50] D.F. Veber, S.R. Johnson, H.-Y. Cheng, B.R. Smith, K.W. Ward, K.D. Kopple, Molecular properties that influence the oral bioavailability of drug candidates, *J. Med. Chem.* 45 (2002) 2615–2623, <https://doi.org/10.1021/jm020017n>.
- [51] I. Muegge, S.L. Heald, D. Brittelli, Simple selection criteria for drug-like chemical matter, *J. Med. Chem.* 44 (2001) 1841–1846, <https://doi.org/10.1021/jm015507e>.
- [52] K.L. Valkó, Lipophilicity and biomimetic properties measured by HPLC to support drug discovery, *J. Pharm. Biomed. Anal.* 130 (2016) 35–54, <https://doi.org/10.1016/j.jpba.2016.04.009>.
- [53] A. Schulze, F. Mitterer, J.P. Pombo, S. Schild, Biofilms by bacterial human pathogens: clinical relevance – development, composition and regulation - therapeutic strategies, *Microb. Cell* 8 (2021) 28–56, <https://doi.org/10.15698/MIC2021.02.741>.
- [54] M.E. Skogman, P.M. Vuorela, A. Fallarero, A platform of anti-biofilm assays suited to the exploration of natural compound libraries, *J. Vis. Exp.* 2016 (2016), e54829, <https://doi.org/10.3791/54829>.
- [55] M.E. Sandberg, D. Schellmann, G. Brunhofer, T. Erker, I. Busygin, R. Leino, P. M. Vuorela, A. Fallarero, Pros and cons of using resazurin staining for quantification of viable staphylococcus aureus biofilms in a screening assay, *J. Microbiol. Methods* 78 (2009) 104–106, <https://doi.org/10.1016/j.mimet.2009.04.014>.
- [56] M.E. Skogman, P.M. Vuorela, A. Fallarero, Combining biofilm matrix measurements with biomass and viability assays in susceptibility assessments of antimicrobials against staphylococcus aureus biofilms, *J. Antibiot.* 65 (2012) 453–459, <https://doi.org/10.1038/ja.2012.49>.
- [57] www.promega.com. (Accessed 1 June 2022).
- [58] M. Oblak, M. Kotnik, T. Šolmajer, Discovery and development of ATPase inhibitors of DNA gyrase as antibacterial agents, *Curr. Med. Chem.* 14 (2007) 2033–2047, <https://doi.org/10.2174/092986707781368414>.
- [59] A. Wohlkonig, P.F. Chan, A.P. Fosberry, P. Homes, J. Huang, M. Kranz, V. R. Leydon, T.J. Miles, N.D. Pearson, R.L. Perera, A.J. Shillings, M.N. Gwynn, B. D. Bax, Structural basis of quinolone inhibition of type IIA topoisomerases and target-mediated resistance, *Nat. Struct. Mol. Biol.* 17 (2010) 1152–1153, <https://doi.org/10.1038/nsmb.1892>.
- [60] K. Drlica, Mechanism of fluoroquinolone action, *Curr. Opin. Microbiol.* 2 (1999) 504–508, [https://doi.org/10.1016/s1369-5274\(99\)00008-9](https://doi.org/10.1016/s1369-5274(99)00008-9).
- [61] K.J. Aldred, R.J. Kerns, N. Osheroff, Mechanism of quinolone action and resistance, *Biochemistry* 53 (2014) 1565–1574, <https://doi.org/10.1021/bi5000564>.
- [62] RCSB Protein Data Bank. <https://www.rcsb.org/>. (Accessed 21 July 2022).
- [63] P.F. Chan, V. Srikannathasan, J. Huang, H. Cui, A.P. Fosberry, M. Gu, M.M. Hann, M. Hibbs, P. Homes, K. Ingraham, J. Pizzollo, C. Shen, A.J. Shillings, C. E. Spitzfaden, R. Tanner, A.J. Theobald, R.A. Stavenger, B.D. Bax, M.N. Gwynn, Structural basis of DNA gyrase inhibition by antibacterial QPT-1, anticancer drug etoposide and moxifloxacin, *Nat. Commun.* 6 (2015), 10048, <https://doi.org/10.1038/ncomms10048>.
- [64] D.A. Veselkov, I. Laponogov, X.-S. Pan, J. Selvarajah, G.B. Skamrova, A. Branstrom, J. Narasimhan, J.V.N.V. Prasad, L.M. Fisher, M.R. Sanderson, Structure of a quinolone-stabilized cleavage complex of topoisomerase IV from *Klebsiella pneumoniae* and comparison with a related *Streptococcus pneumoniae* complex, *Acta Crystallogr. D. Struct. Biol.* 72 (2016) 488–496, <https://doi.org/10.1107/S2059798316001212>.
- [65] Release 4.1.2.2, OpenEye Scientific Software, Inc., Santa Fe, NM, USA; www.eyesopen.com.
- [66] E.Y. Ng, M. Trucksis, D.C. Hooper, Quinolone resistance mediated by norA: physiologic characterization and relationship to flqB, a quinolone resistance locus on the *Staphylococcus aureus* chromosome, *Antimicrob. Agents Chemother.* 38 (1994) 1345–1355.
- [67] H. Nikaido, D.G. Thanassi, Penetration of lipophilic agents with multiple protonation sites into bacterial cells: tetracyclines and fluoroquinolones as examples, *Antimicrob. Agents Chemother.* 37 (1993) 1393–1399.
- [68] J.S. Chapman, N.H. Georgopapadakou, Routes of quinolone permeation in *Escherichia coli*, *Antimicrob. Agents Chemother.* 32 (1988) 438–442.
- [69] A.J.H. Marshall, L.J.V. Piddock, Interaction of divalent cations, quinolones and bacteria, *J. Antimicrob. Chemother.* 34 (1994) 465–483.
- [70] G.E. Schulz, The structure of bacterial outer membrane proteins, *Biochim. Biophys. Acta* 1565 (2002) 308–317, [https://doi.org/10.1016/S0005-2736\(02\)00577-1](https://doi.org/10.1016/S0005-2736(02)00577-1).
- [71] H. Nikaido, Molecular basis of bacterial outer membrane permeability revisited, *Microbiol. Mol. Biol. Rev.* 67 (2003) 593–656, <https://doi.org/10.1128/MMBR.67.4.593-656.2003>.
- [72] J.M. Pages, C.E. James, M. Winterhalter, The porin and the permeating antibiotic: a selective diffusion barrier in Gram-negative bacteria, *Nat. Rev. Microbiol.* 6 (2008) 893–903, <https://doi.org/10.1038/nrmicro1994>.
- [73] J. Sączewski, K. Hinc, M. Obuchowski, M. Gdaniec, The tandem Mannich – electrophilic amination reaction: a versatile platform for fluorescent probing and labeling, *Chem. Eur J.* 19 (2013) 11531–11535, <https://doi.org/10.1002/chem.201302085>.
- [74] J. Sączewski, J. Fedorowicz, M. Korcz, F. Sączewski, B. Wicher, M. Gdaniec, A. Konopacka, Experimental and theoretical studies on the tautomerism and reactivity of isoxazolo[3,4-b]quinolin-3(1H)-ones, *Tetrahedron* 71 (2015) 8975–8984, <https://doi.org/10.1016/j.tet.2015.09.050>.
- [75] Agilent Technologies: *CrysAlisPRO Software System*, Agilent Technologies UK Ltd, Oxford, UK, 2014. *Version 1.171.37.35g*.
- [76] G.M. Sheldrick, SHELXT – integrated space-group and crystal-structure determination, *Acta Crystallogr. A. Found. Crystallogr.* 71 (2015) 3–8, <https://doi.org/10.1107/S2053273314026370>.
- [77] G.M. Sheldrick, Crystal structure refinement with SHELXL, *Acta Crystallogr. C. Struct. Chem.* 71 (2015) 3–8, <https://doi.org/10.1107/S2053229614024218>.
- [78] L.J. Faruggia, WinGX suite for small-molecule single-crystal crystallography, *J. Appl. Crystallogr.* 32 (1999) 837–838, <https://doi.org/10.1107/S0021889899006020>.
- [79] F.H. Allen, The Cambridge Structural Database: a quarter of a million crystal structures and rising, *Acta Crystallogr. B. Struct. Sci. Cryst. Eng. Mater.* 58 (2002) 380–388, <https://doi.org/10.1107/s0108768102003890>.
- [80] CLSI, *Methods for Dilution Antimicrobial Susceptibility Tests for Bacteria that Grow Aerobically*; Approved Standard, 10 ed., Clinical and Laboratory Standards Institute, 2015.
- [81] <http://www.swissadme.ch>. (Accessed 1 June 2022).
- [82] M.R. McGann, H.R. Almond, A. Nicholls, J.A. Grant, F.K. Brown, Gaussian docking functions, *Biopolymers* 68 (2003) 76–90, <https://doi.org/10.1002/bip.10207>.
- [83] G.B. McGaughey, R.P. Sheridan, C.I. Bayly, J.C. Culbertson, C. Kretsoulas, S. Lindsley, V. Maiorov, J.F. Truchon, W.D. Cornell, Comparison of topological, shape, and docking methods in virtual screening, *J. Chem. Inf. Model.* 47 (2007) 1504–1519, <https://doi.org/10.1021/ci700052x>.
- [84] Release 4.2.0.1, OpenEye Scientific Software, Inc., Santa Fe, NM, USA; www.eyesopen.com.
- [85] P.C.D. Hawkins, A.G. Skillman, G.L. Warren, B.A. Ellingson, M.T. Stahl, Conformer generation with OMEGA: algorithm and validation using high quality structures from the Protein Databank and Cambridge Structural Database, *J. Chem. Inf. Model.* 50 (2010) 572–584, <https://doi.org/10.1021/ci100031x>.